

Research paper

CFD simulation of multiple moored floating structures using OpenFOAM: An open-access mooring restraints library

Haifei Chen ^{a,*}, Tanausú Almeida Medina ^{b,c}, Jose Luis Cercos-Pita ^c^a Interdisciplinary Science Cooperative, University of New Mexico, Albuquerque, NM, 87131, USA^b Universidad da Coruña, Campus Industrial de Ferrol, CITENI, Spain^c Coremarine Solutions SL, Madrid, Spain

ARTICLE INFO

Keywords:

Wave-structure interaction
Rigid body dynamics
OpenFOAM
Overset
Mooring dynamics
Underwater towed system

ABSTRACT

It is not uncommon to observe multiple floating structures in proximity in the coastal and ocean environments. Individually moored or interconnected through hinges or shared mooring lines, these structures can be constructed to form an offshore floating wind farm, a wave energy converter array, or an aquaculture farm. This paper presents the development and application of a Computational Fluid Dynamics model coupled with mooring analysis codes to simulate the dynamic response of multiple moored floating structures. Both the six degrees of freedom rigid body motion library and the multibody dynamics library in the open-source finite volume CFD toolbox, OpenFOAM, are extended with a quasi-static mooring model and two dynamic mooring models. The overset grid method is adopted to account for the mesh motions of multiple rigid bodies. The coupled CFD-mooring model is validated against experimental measurements for a single box-type floating breakwater and a twin floating breakwater moored in regular waves, as well as the steady-state postures of an underwater towed system. The coupled model is also verified by comparing OpenFOAM results with those of a Smoothed Particle Hydrodynamics solver. The mooring restraints library developed in this work, foamMooring, is open-source and can be applied to simulate the multibody systems involved in emerging offshore wind and wave energy technologies and open ocean aquaculture farms.

1. Introduction

A plethora of floating structure systems have been designed to serve the purposes of various offshore industries, some of which may operate in harsh environments and thus withstand the extreme loads of strong winds, waves, and currents. A robust mooring system is typically an indispensable component of these systems to ensure the integrity of the structures and the safety of life at sea. In order to reduce a project's total cost of construction, installation, operation, and maintenance, one may resort to scaling up an individual structure to an array of structures, with or without inter-body connections. Typical application scenarios of these floating systems include Wave Energy Converter (WEC) arrays ([da Fonseca et al., 2016](#); [Gomes et al., 2020](#)), offshore wind farms ([Lopez-Olocio et al., 2023](#); [Lozon and Hall, 2023](#)), aquaculture farms ([Fredriksson et al., 2004](#); [Ma et al., 2022](#)), and even multi-use platforms. [Li et al. \(2020\)](#) proposed a framework to assess the technical feasibility of a multi-purpose platform which is comprised of a wind turbine, an array of WECs, and an internal pool to accommodate aquaculture fish cages. In

contrast to conventional offshore oil & gas applications, where mooring systems typically represent a smaller portion of project costs, emerging wind and wave energy technologies often allocate a significant share of expenses to mooring systems. Consequently, minimizing loads and costs is a notable challenge to overcome, particularly in the context of WECs, where optimization requires maximizing motions ([Xu et al., 2019](#)). Along this line, compact WEC arrays and wind farms with shared moorings can potentially reduce the leveled cost of energy. Recent experimental campaigns ([Gomes et al., 2020](#); [Howey et al., 2021](#); [Lopez-Olocio et al., 2023](#)) highlight the potential challenges faced by the shared mooring system design for these emerging technologies.

Design and analysis of these floating structure systems is normally conducted using experimentally validated numerical models. Currently the dominant models are based on the potential flow theory, with the hydrodynamics solved by a diffraction-radiation code and the system response solved in either the frequency domain which captures only the linear steady state solution or the time domain which captures the nonlinear and transient dynamics ([Jin et al., 2020, 2023](#); [Jiang et al.,](#)

* Corresponding author.

E-mail address: hfchen@unm.edu (H. Chen).

2023; Zeng et al., 2024; Zheng et al., 2015). For individually moored multiple bodies without internal connections, the system's equations of motion are straightforward extensions of the equation of motion of a single body. Each body's six-degree-of-freedom (six-DoF) motions can be solved independently. For multiple bodies interconnected with shared moorings, it is also relatively easy to solve the equation of motion for each body, except that the body response and the shared moorings need to be solved implicitly together or explicitly by iteration. Oikonomou et al. (2020) presented a frequency domain analysis of a triangular array of spar-buoy OWC devices. Their results showed that the performance of the independently moored array and the array with inter-body mooring connections were similar, suggesting a positive park effect under a realistic wave climate. Lozon and Hall (2023) explored the dynamics of a 10-turbine shared-mooring floating wind array using wind farm simulator FAST.Farm. The results showed that the shared-mooring design has smaller fluctuations in surge when compared to the baseline array of individually moored turbines. It was concluded that the shared moorings did not overall introduce any dynamic response concerns in their floating wind array design.

For multiple bodies connected with kinematic constraints such as hinges/joints, their dynamics is described by the equations of motion of the bodies and the constraint equations at the connections. Many numerical models have been developed by combining a potential flow hydrodynamics solver with Lagrange multiplier or mode expansion technique to account for hydrodynamic interactions among bodies and the mechanical coupling effect of the hinges (Jin et al., 2023; Zheng et al., 2015). Zhang et al. (2023) extended an in-house potential flow code with the Lagrange multiplier technique to investigate the motion responses of a large array of modularized hinged bodies. The frequency domain method was validated through a 5-box array physical test, which was then applied to examine the effects of the hinge constraints, the number of longitudinal modules, and the external stiffness constraints. It was revealed that the motion responses of a hinged array were highly sensitive to the external constraints such as mooring lines. Instead of using conventional in-house code, Jin et al. (2023) assessed the application of open-source tool WEC-Sim (Wave Energy Converter SIMulator) to model a two-body hinged raft WEC. Developed in MATLAB/Simulink using the multi-body dynamics solver Simscape Multi-body, WEC-Sim can model devices that are comprised of hydrodynamic bodies, joints and constraints, power take-off systems, and mooring systems (WEC-Sim). Two corrections concerning wave excitation force and body-body radiation force were made, and a physically validated viscous term was added to the updated time-domain model to improve the modelling accuracy.

Compared to the potential flow theory-based models, it is rare to see Computational Fluid Dynamics (CFD) models applied to simulate multiple floating structures. CFD models solves the Navier-Stokes equations directly. Combined with a rigid body dynamics solver, they can account for fluid viscosity, turbulence, wave breaking, green water, slamming/impact, and overtopping that are all elusive in the potential flow models. Computationally expensive, these high-fidelity models can provide empirical damping coefficients that are usually required in potential flow models (Han et al., 2023; Jin et al., 2023). Most CFD investigations of floating structures are currently focusing on a single body (Chen and Hall, 2022; Huang et al., 2022), and those simulating multiple structures are restricted to motions in specific degrees of freedom only (Devolder et al., 2018; Han et al., 2023; Jiang and el Moctar, 2023). He et al. (2022) investigated multi-body hydrodynamic interaction between an octagonal platform and absorber-type WECs utilizing StarCCM+. Li et al. (2022) developed a numerical modeling tool coupling OpenFOAM and Multi-body Dynamics code (MBDyn) to resolve the mechanical interaction among sub-structures in a WEC array. Wei et al. (2024) integrated a quasi-static mooring module into a similar model to investigate the coupling effects between the mooring system and the hydroelasticity of Very Large Floating Structures (VLFSs) in waves. A number of CFD studies have recently investigated the effect of the

upstream structure's motion on the gap resonance that is occurring in a narrow gap between multiple structures (Gao et al., 2021, 2022; Jing et al., 2024).

A couple of Smoothed Particle Hydrodynamics (SPH) solvers have also been developed to simulate multibody hydrodynamics. Chen et al. (2023) studied the hydrodynamics of a twin individually moored floating breakwater (FB) using δ -SPH coupled with a catenary theory based mooring line model. He et al. (2023) established an SPH model to simulate a hinged multi-float structure, which is restrained by linear springs and has rubber bumpers equipped to absorb the collision energy between adjacent modules. Both of the SPH studies are validated against experimental measurements, which could be used to validate other numerical models. Domínguez et al. (2019) is the first of its kind to enable SPH flow solvers to simulate floating structures with mooring dynamics. A lumped-mass mooring model (Hall and Goupee, 2015) is especially adapted to simulate multiple floating structures with individual moorings or shared moorings.

The aim of the present paper is to develop and validate a coupled CFD-mooring model to simulate the dynamic response of multiple moored floating structures. The coupled model is implemented in the leading open-source CFD toolbox, OpenFOAM, the modular structure of which makes it easy to extend the code's functionalities (Weller et al., 1998). There are two libraries in OpenFOAM that can handle floating body motions: *sixDoFRigidBodyMotion* and *rigidBodyMotion*. The former solves directly the six-DoF motion of a rigid body, while the latter is specially implemented to solve the multibody dynamics involved in WEC applications. In this paper, both libraries are extended with an open-source mooring restraint library, *foamMooring*, which provides an interface to a lumped-mass mooring model MoorDyn (Hall and Goupee, 2015), a quasi-static mooring model MAP++ (Masciola et al., 2013), and a finite element model Moody (Palm et al., 2017). Fig. 1 shows how the new library incorporates the functionalities of the three mooring codes into the two rigid body motion solvers in the same CFD toolbox. Thanks to recent developments of MoorDyn, the coupled CFD-mooring model developed in Chen and Hall (2022), which adopted the *sixDoFRigidBodyMotion* library, can now be applied to simulate multiple individually moored bodies.

Many mooring line models have been developed over the decades, which can be generally categorized into quasi-static models and dynamic models. The most widely adopted dynamic models are based on either a finite element or lumped-mass formulation. To enable researchers a greater altitude of developing a customized CFD-mooring model, the present study focused on open-source mooring models. According to a recent comparison study among three quasi-static models and three dynamic models Zhong et al., (2024), MoorDyn and Moody are the two mooring models recommended for coupled FWT-mooring simulations. Moody may be more computationally efficient because of its high-order finite element formulation. However, the relative efficiency of the in-house Moody versus the open-source MoorDyn may be eclipsed in the face of the enormous computational demand of CFD simulations. Being now a community project, MoorDyn boasts some unique capabilities such as mooring line failure modeling and changing cable length during simulations.

It should be noted that there are already OpenFOAM applications to simulate multiple floating structures. Chen et al. (2022) used a coupled OpenFOAM and dynamic mooring model to study the wave dissipation performance of a single FB and a twin FB under long-period waves. The numerical model (presumably using *rigidBodyMotion* library) was validated using experimental data for a single FB in terms of the wave transmission coefficient, motion and tension amplitude; results for the twin FB were presented without experimental validation. Eskilsson and Palm (2022) extended the six-DoF rigid body motion solver with a finite element mooring model to simulate interconnected multiple bodies, specifically mooring components such as submerged buoys and clump weights. Jiang and el Moctar (2023) extended the *rigidBodyMotion* library with a mooring model to simulate hinged multiple bodies. Both

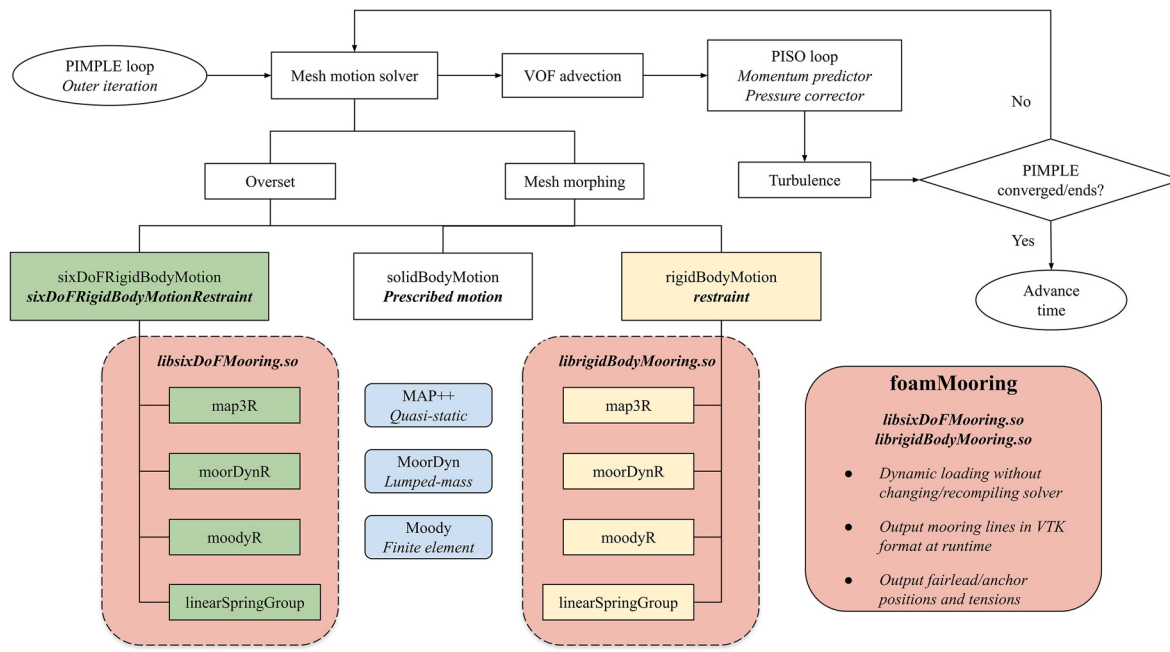


Fig. 1. The mooring restraints library, *foamMooring*, in the context of a flowchart for CFD simulation of moored rigid body motions using OpenFOAM's two-phase flow solver.

latter studies adopted the mesh morphing technique to accommodate the body motions, which may not be adequate when the body motions are significant (Chen and Hall, 2022).

Taking FB as an example of multiple moored floating structures, the present study develops and validates a coupled CFD-mooring model against time series of experimental measurements for a twin FB moored in regular waves. This contribution extends the rigid body motion libraries in OpenFOAM, thus enabling high-fidelity simulations of floating structure systems that are emerging in the wind and wave energy technologies. It is believed that this study is the first of its kind to take advantage of the most recent developments of the lumped-mass mooring model, MoorDyn, which now supports (de-) serialization of the mooring system state at each time step and runtime generation of visualization files for the mooring system. To encourage reproducible open research and further application to more complex floating structure systems, the mooring restraint library is released open source. The case studies presented in this paper may serve as a valuable verification and validation exercise for OpenFOAM and other CFD models.

The remainder of the paper is structured as follows. Section 2 describes the various components of the coupled model, including free surface flow solver, rigid body motion solver, mesh motion solver, mooring lines model, and the coupling procedure between the flow solver, the body motion solver, and the mooring models. Section 3 presents three case studies validating the coupled CFD-mooring model: a single FB (Section 3.1), a twin FB (Section 3.2), and an underwater towed system (Section 3.3). The overset grid method is used as the mesh motion solver for multiple bodies. The numerical results from the two rigid body motion solvers in OpenFOAM are also compared with those by a meshless SPH solver, DualSPHysics. A simulation of a twin FB with shared moorings is demonstrated as well. Section 4 summarizes the conclusions of this study.

2. Methodology

2.1. Two-phase flow solver

The air-water mixture based two-phase flow solver in OpenFOAM solves the Reynolds-Averaged Navier-Stokes (RANS) equations for two incompressible phases using a finite volume discretization and the

Volume of Fluid (VOF) surface capturing method (Jasak, 1996; Rusche, 2002). The governing equations describing mass continuity and conservation of momentum for an incompressible fluid are given by

$$\nabla \bullet \mathbf{U} = 0 \quad (1)$$

$$\frac{\partial \rho \mathbf{U}}{\partial t} + \nabla \bullet (\rho(\mathbf{U} - \mathbf{U}_g)\mathbf{U}) - \nabla \bullet (\mu_{\text{eff}} \nabla \mathbf{U}) = -\nabla p^* - \mathbf{g} \bullet \mathbf{X} \nabla \rho + \nabla \mathbf{U} \bullet \nabla \mu_{\text{eff}} \quad (2)$$

where \mathbf{U} is fluid velocity vector in Cartesian coordinates, ρ density of the mixed fluid, \mathbf{U}_g grid velocity to account for the moving or deforming grids, $p^* = p - \rho \mathbf{g} \bullet \mathbf{X}$ pseudo-dynamic pressure, p total pressure, \mathbf{g} acceleration due to gravity, \mathbf{X} position vector of the computational cells, and $\mu_{\text{eff}} = \mu + \mu_t$ effective dynamic viscosity, which is the sum of molecular dynamic viscosity μ and turbulent dynamic viscosity μ_t . A variety of turbulence models are available in OpenFOAM. But for the case studies presented in this study which have simple body geometries, no turbulence modelling is switched on. Activating turbulence modelling is not expected to alter significantly the numerical results, as demonstrated in Chen and Hall (2022) and other many other similar mesh-based CFD studies of wave-structure interactions, as well as the apparent absence of turbulence models in SPH simulations of floating structures (e.g., Domínguez et al., 2019; Chen et al., 2023; He et al., 2023). Even though the turbulence models are not switched on and the boundary layers may not be resolved accurately, the wave force contribution due to the viscous shear can still be accounted for to some extent. For floating structures in close proximity where gap resonance occurs, a couple of CFD studies using OpenFOAM have resorted to laminar flow models only (Feng et al., 2017; Gao et al., 2021, 2022). Specifically, Feng et al. (2017) reported that turbulence models had no effects on their numerical results for the gap resonance between side-by-side boxes/barges.

The free surface is captured by solving transport equation

$$\frac{\partial \alpha}{\partial t} + \nabla \bullet (\mathbf{U}\alpha) + \nabla \bullet (\mathbf{U}_t \alpha(1 - \alpha)) = 0 \quad (3)$$

in which α is volume fraction of water in a computational cell and \mathbf{U}_t is an artificial compressive velocity field normal to the interface. Note that an extra term is added to limit the smearing of air-water interface (Hirt

and Nichols, 1981). This convective term is active only in the vicinity of the interface $0 < \alpha < 1$, where the cells are occupied by a mixture of the two fluids. The smaller the cell size, the thinner the air-water interface. The density ρ and the viscosity μ of the mixture in each cell are α -weighted average of those of air and water. In this algebraic VOF, the location of the air-water interface can be approximated by taking an iso-surface of $\alpha = 0.5$ in the interface cells. More details about the VOF method can be found in Rusche (2002).

2.2. Rigid body motion

Both the six-DoF motion library, *sixDoFRigidBodyMotion*, and the multibody dynamics library, *rigidBodyMotion*, are used to solve the motions of multiple floating structures. For multiple bodies without internal connections, each body's six-DoF motions can be treated separately based on the Newton's second law:

$$\frac{d\mathbf{v}_f}{dt} = \mathbf{F}_f/m_f \quad (4)$$

$$\frac{d\omega_f}{dt} = \mathbf{I}_f^{-1} \bullet (\mathbf{M}_f - \omega_f \times (\mathbf{I}_f \bullet \omega_f)) \quad (5)$$

where the subscript f denotes the quantities for the floating body. \mathbf{v}_f and ω_f are the linear and angular velocity of the body, and m_f and \mathbf{I}_f are the mass and moment of inertia of the body. \mathbf{F}_f and \mathbf{M}_f are the total external forces and moments acting on the body, which includes the gravity, the fluid force, and the mooring restraint force. The fluid forces are calculated by integrating the normal pressure and the tangential shear stress over all the patches enclosing the body (Gatin et al., 2017). The mooring force is calculated using one of the mooring restraints to be described in Section 2.4.

The native rigid body motion library in OpenFOAM, i.e. *sixDoFRigidBodyMotion*, is applied to solve the six-DoF motions for each of the floating bodies. The hydrodynamic forces/moment acting on the body are first calculated, which gives an initial acceleration for each new iteration or time step. All the restraining forces/moment are then requested from all instances of *sixDoFRigidBodyMotionRestraint* in order to update the body's acceleration. Once the linear and angular accelerations are obtained, the Newmark $-\beta$ integration scheme is applied to update the velocity, position, and orientation of the floating body. Note that the linear and angular accelerations are solved separately using 3D vector equations.

For multiple bodies loosely connected by shared moorings, towing cables, or those constrained with kinematic joints, one has to resort to the rigid body dynamics library, *rigidBodyMotion*, to solve their motions. Following Featherstone (2014), 6D vectors are used to combine the linear and angular aspects of rigid-body motions and forces. For example, linear and angular velocity are combined to form a spatial velocity vector; force and moment are combined to form a spatial force vector. This provides a compact notation for studying rigid-body dynamics. Using an angular-before-linear spatial notation, the two 3D vector equations of motion, Eqs. (4) and (5), for a rigid body can be written as

$$\mathbf{f} = \mathbf{I}\dot{\mathbf{a}} + \mathbf{v} \times^* \mathbf{I}\mathbf{v} \quad (6)$$

$$\mathbf{f} = (\mathbf{M}_f, \mathbf{F}_f) \quad (7)$$

$$\mathbf{v} = (\omega_f, \mathbf{v}_f) \quad (8)$$

$$\mathbf{a} = (\dot{\omega}_f, \dot{\mathbf{v}}_f - \omega_f \times \mathbf{v}_f) \quad (9)$$

$$\mathbf{I} = \begin{bmatrix} \mathbf{I}_f & \mathbf{0} \\ \mathbf{0} & m_f \mathbf{I}_3 \end{bmatrix} \quad (10)$$

where \mathbf{f} is the spatial force acting on the body, \mathbf{v} and \mathbf{a} are the body's spatial velocity and acceleration, \mathbf{I}_3 is identity matrix of size 3, and \mathbf{I} is

the body's spatial inertia tensor. The symbol \times^* in Eq. (6) denotes a spatial vector cross product.

For a rigid-body system containing multiple rigid bodies and joints, the equations of motion expressed in generalized (joint-space) coordinates can be written in the following form

$$\mathbf{H}(\mathbf{q})\ddot{\mathbf{q}} + \mathbf{C}(\mathbf{q}, \dot{\mathbf{q}}) = \boldsymbol{\tau} \quad (11)$$

where \mathbf{q} , $\dot{\mathbf{q}}$ and \mathbf{q} are vectors of generalized (joint) position, velocity, and acceleration variables, respectively, \mathbf{H} is generalized inertia matrix, \mathbf{C} is generalized bias force, and $\boldsymbol{\tau}$ is a vector of generalized forces. The bias force is simply the value of $\boldsymbol{\tau}$ that produces zero acceleration. It accounts for the Coriolis and centrifugal forces, gravity, and any other forces (hydrodynamic and mooring force in this study) acting on the system other than those in $\boldsymbol{\tau}$.

The rigid body dynamics library in OpenFOAM implemented the articulated-body algorithm for forward dynamics problems

$$\ddot{\mathbf{q}} = \text{FD}(\text{model}, \mathbf{q}, \dot{\mathbf{q}}, \boldsymbol{\tau}) \quad (12)$$

which aims to calculate the acceleration response of a rigid-body system to any applied forces. The symbol *model* in Eq. (12) refers to a collection of data that describes a particular rigid-body system: the number of bodies and joints, their connectivity, the values of every parameter associated with each component such as inertia and geometric parameters (Featherstone, 2014). While the built-in six-DoF motions solver calculates the body motion one by one, this multibody dynamics solver calculates the motion responses of all bodies together. After the hydrodynamic forces/moment acting on all the bodies are calculated, the reacting forces/moment by all restraints are added up to the body each of the restraint is attached to. The forward dynamics algorithm then calculates the joint acceleration from the joints state and forces. The joints velocity and position are then integrated using the Newmark $-\beta$ scheme. The bodies state is finally updated to correspond to the current joints state. This algorithm is inherently applicable to simulations of interconnected bodies and multiple hinged bodies.

2.3. Mesh motion

The overset mesh library in OpenFOAM (v2212) is particularly suitable for applications involving large-amplitude body motions and multiple moving bodies (Chen et al., 2019). In the overset mesh method, two sets of grids are defined: a relatively large background grid and a set of local overset grids each enclosing one of the moving bodies. A composite computational domain is then generated via cell-to-cell mappings between the two sets of disconnected grids, which overlap each other. The background grid is mostly stationary, while the overset grid moves following the body motion, prescribed in advance or calculated using the two rigid body motion libraries in OpenFOAM (see Fig. 1). All the computational cells in the CFD domain are classified into three categories: *calculated*, *interpolated*, and *holes*. The flow governing equations are solved for *calculated* cells. The *interpolated* cells are used to interpolate flow variables between the two mesh regions. The *holes* cells, which represent the moving body, are blocked out during the calculation. Because of the interpolation between different mesh regions, the overset mesh method may be more computationally demanding than the mesh deformation method (Chen and Hall, 2022). It is recommended to use similar background and overset grid cell sizes in the vicinity of the overset patch in order to reduce the interpolation error and speed up the overset grid computation.

2.4. Mooring line models

Three mooring analysis codes, a quasi-static mooring model MAP++ (Mascioli et al., 2013), a lumped-mass mooring model MoorDyn (Hall and Goupee, 2015), and a finite element model Moody (Palm et al., 2017), are coupled with OpenFOAM's rigid body motion solvers by

Table 1

Main parameters of laboratory-scale floating breakwaters (FB).

Parameters	Single FB (Liang et al., 2022)	Twin FB (Chen et al., 2023)
Breakwater		
Length (m)	0.745	0.745
Breadth (m)	0.5	0.5
Height (m)	0.28	0.3
Draft (m)	0.16	0.15
Mass (kg)	58.09	55.875
Moment of inertia ($\text{kg}\cdot\text{m}^2$)	2.441	2.208
Center of gravity above bottom (m)	0.0652	0.0729
Mooring lines		
Length (m)	0.809	0.62
Density (kg/m)	0.177	0.177
Spring stiffness (kN/m)	2.36	2.6
Water depth (m)	0.6	0.514
Wave height (m)	0.1	0.05
Wave period (s)	1.4	1.4, 1.7, 2.0

developing three corresponding rigid body motion restraints. Herein only an overview of the three mooring models is provided. Readers are referred to the original references for detailed implementations of the models. Table 1 in Chen and Hall (2022) listed the main features of the three mooring analysis codes. Both MAP++ and MoorDyn are open-source, with the latter under continuous development. Moody is an in-house code but a precompiled library is released for coupling with other codes. MAP++ is a quasi-static mooring model based on an extension of conventional single line catenary solutions, allowing multi-line mooring systems with arbitrary connections to be analyzed. MoorDyn is a lumped-mass mooring analysis library. Each mooring line is discretized into a number of equal-length segments, each segment connecting two neighboring nodes. All the line mass and external forces acting on the line, including buoyancy, seabed contact force, and hydrodynamic drag and inertia forces based on Morison's equation, are lumped at a finite number of nodes. Massless springs are conceived to connect the adjacent nodes representing the internal tension and damping forces. The lumped-mass formulation solves the equations of motion for each node i which has a global coordinate position vector \mathbf{r}_i .

$$(m_i \mathbf{I}_3 + \mathbf{a}_{ni} + \mathbf{a}_ti) \ddot{\mathbf{r}}_i = \mathbf{T}_i + \mathbf{C}_i + \mathbf{W}_i + \mathbf{B}_i + \mathbf{D}_{ni} + \mathbf{D}_{ti} \quad (13)$$

where m_i is the point mass which is half the combined mass of all line segments connected with the node, $\ddot{\mathbf{r}}_i$ the node's acceleration, \mathbf{T}_i , \mathbf{C}_i the internal tension and damping resultant force from the node's connecting segments, \mathbf{W}_i , \mathbf{B}_i the submerged weight and seabed contact force, \mathbf{D}_{ni} , \mathbf{D}_{ti} the transverse and tangential components of the drag force, and \mathbf{a}_{ni} , \mathbf{a}_ti are the transverse and tangential components of the added mass matrix. A new version of MoorDyn (v2) enables its use for an array of floating structures with and without shared mooring lines (Lozon and Hall, 2023).

Moody is a finite element mooring dynamics model developed with the special intent of capturing and resolving snap loads (Palm et al., 2017). Unlike the lumped-mass formulation, this model is derived first and foremost from the governing equations of motion for an elastic cable

$$\gamma_0 \ddot{\mathbf{r}} = \frac{\partial}{\partial s} (T \hat{\mathbf{t}}) + \mathbf{f} \quad (14)$$

$$\hat{\mathbf{t}} = \frac{\partial \mathbf{r}}{\partial s} \left| \frac{\partial \mathbf{r}}{\partial s} \right|^{-1} \quad (15)$$

$$T = EA \left(\left| \frac{\partial \mathbf{r}}{\partial s} \right| - 1 \right) \quad (16)$$

where \mathbf{r} and $\ddot{\mathbf{r}}$ are global coordinate position vector and acceleration of the cable, s curvilinear coordinate along the cable, γ_0 mass per unit length, $\hat{\mathbf{t}}$ tangent unit vector along the arclength s , T tension force magnitude, EA axial stiffness assuming a linear elastic cable material,

and \mathbf{f} all the external forces consisting of the added mass and Froude-Krylov force, the viscous drag force, the net force of gravity and buoyancy, and the seabed contact force. The governing equations are then discretized using an hp -adaptive discontinuous Galerkin method. The high-order formulation ensures engineering accuracy can be achieved using only a few elements.

2.5. Coupling CFD with mooring models

The coupling of floating body motion with two-phase free surface flows is accomplished with a PIMPLE loop implemented in OpenFOAM's flow solvers, which is a combination of SIMPLE and PISO algorithms. For each PIMPLE iteration (Fig. 1), the floating body motion is solved first and the mesh motion updated. The VOF transport equation is then solved to advect the air-water interface. The pressure-velocity coupling is resolved with a PISO loop, which consists of one optional momentum predictor and several pressure corrections. The PIMPLE loop within each time step may alleviate the time lag between and thus converge the flow and the body motion. More tightly coupled CFD and body motion solvers may be needed to enhance this partitioned approach (Dunbar et al., 2015; Gatin et al., 2017; Bruinsma et al., 2018).

The coupling of the mooring models with floating body motion solver follows a loose-coupling approach. Several mooring restraints are developed in *foamMooring* package to complement the two rigid body motion libraries *sixDoFRigidBodyMotion* and *rigidBodyMotion* in OpenFOAM (Fig. 1). Two coupling modes, i.e., body coupling and point coupling, are proposed to indicate whether the body-mooring coupling is achieved via either the body's center of gravity (rotation) or the mooring lines' attachments points (fairleads) on the body. For all three mooring models, the mooring system is initialized when the mooring forces are requested via the body motion solver for the first time.

For body coupling, the position and velocity of the floating body are passed from the body motion solver to the mooring restraint, which updates the fairlead kinematics and the mooring system states such as the mooring line nodes' position, velocity, and tension. The mooring model then calculates the total restraining forces and moments acting on the floating body by summing all mooring line contributions. The summed forces and moments are returned to the body motion solver to update the body acceleration. For point/fairlead coupling, the mooring attachments positions (calculated from the instantaneous orientation of the floating body) are passed to the mooring models to update the mooring system states. Correspondingly, instead of the total mooring forces/moments exerting on the body, the fairlead tensions from all the mooring lines are returned from the mooring model to the rigid body restraint. The restraint then sums up the total mooring forces/moment and passes them to the motion solver to update the body motion.

The new mooring restraints are compiled into two dynamic libraries (*libsixDoFMooring.so* and *librigidBodyMooring.so*) that can be simply

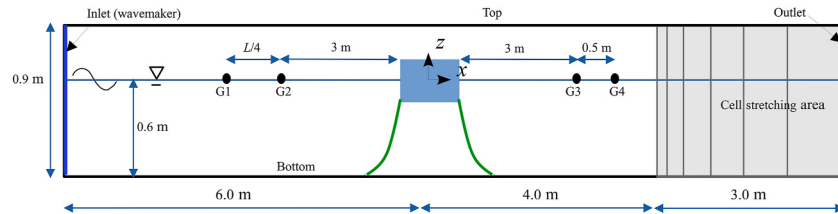


Fig. 2. Numerical model setup for the physical experiment of a box-type floating breakwater (Liang et al., 2022). L is the incident wave length.

loaded at runtime into the built-in OpenFOAM solvers *interFoam* and *overInterDyMFoam*, or into other variants (such as *waveFoam* and *olaFlow*) developed by the community. For the *sixDoFRigidBodyMotion* restraint, both point and body coupling should work equally. However, only the MoorDyn mooring restraint is equipped with both coupling modes at the moment. MAP++ by itself does not calculate the total mooring forces/moments acting on the body. Moody's in-house code was designed to support both coupling modes. But the pre-compiled library does not support debugging the issues encountered with the body coupling approach (see Appendix C). Thanks to MoorDyn's continuous developments, more than one mooring system instance can now be created (Lozon and Hall, 2023). This makes it possible to simulate an array of individually moored floating structures using the built-in *sixDoFRigidBodyMotion* library. To enable simulation of interconnected multiple bodies, a significant rewrite of the library is deemed necessary (Eskilsson and Palm, 2022). For the *rigidBodyMotion* restraints, only the point coupling mode is valid at the time of writing, as the mooring restraining moments requested by the multibody dynamics formulation should be in the global coordinate system. It should be noted that the point coupling mode is more universal and can be applied to simulations of interconnected floating bodies.

3. Results

Three case studies are presented to validate the coupled CFD-mooring model: a single FB, a twin FB, and an underwater towed system. In Section 3.1, the coupled model is validated against experimental tests for a single box-type FB. In Section 3.2, the coupled model is validated against experimental tests for a twin FB, which are individually moored by four catenary lines. A simulation of a twin FB with shared moorings is demonstrated as well. In Section 3.3, the coupled model is validated against the steady-state position and posture of an underwater towed system under four towing speeds.

3.1. A box-type floating breakwater

The extended two rigid body motion solvers are first validated by a box-type floating breakwater moored in regular waves. It should be noted that the new mooring restraint library developed for the *rigidBodyMotion* library is also tested using the floating box experiment studied in Chen and Hall (2022), in which the single box motion was solved using the *sixDoFRigidBodyMotion* library. No differences are observed between the surface elevations, body motions, and mooring line tensions predicted by the two methods. These results are omitted here for the sake of brevity. Interested readers could refer to the tutorial (link provided in acknowledgement) to reproduce the test.

3.1.1. Numerical model setup

The box-type floating breakwater, made of 15 mm thick acrylic plates, is 0.745 m long, 0.5 m wide, and 0.3 m high (Liang et al., 2022). The mass and moment of inertia are 58.09 kg and 2.441 kg·m², respectively. The model draft was adjusted to 0.16 m through steel ballast fixed at the bottom of the breakwater. A four-line catenary mooring system was used to restrain the breakwater. Each mooring line was made of stainless steel with a line density of 0.177 kg/m. The upper

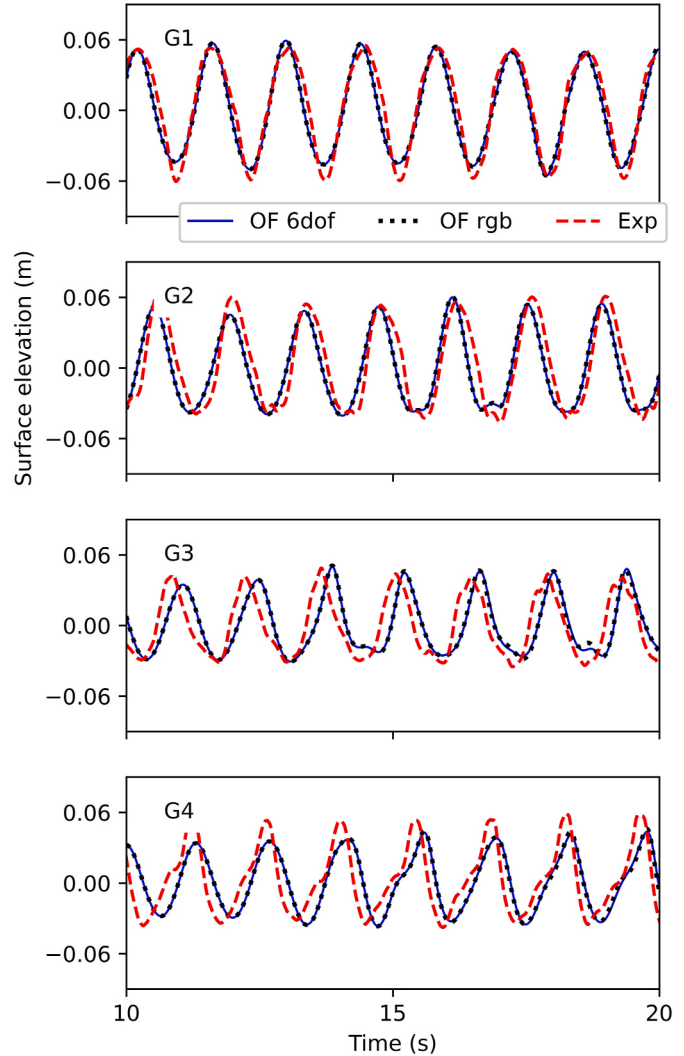


Fig. 3. Numerical and experimental results of surface elevations for the single FB test (wave height 0.1 m and period 1.4 s). OF 6dof: OpenFOAM simulation using six-DoF motion library; OF rgb: OpenFOAM simulation using rigid body dynamics library; Exp: experimental data (Liang et al., 2022).

end of the mooring line is connected to the bottom of the floating breakwater, and a spring was inserted near the top end to simulate the stiffness of the mooring chain with a coefficient of 2.36 kN/m. The lower end was anchored to the flume bottom. The horizontal distance between the two attachment points is 0.639 m. The total length of the mooring line is 0.809 m.

Fig. 2 shows the OpenFOAM model setup for the box-type floating breakwater experiment (Liang et al., 2022), which is bounded by four boundary patches named inlet, outlet, top, and bottom. The 2D numerical flume is 13 m long and 0.9 m high. The still water depth is 0.6 m. As in the physical experiments, four wave gauges (denoted G1, G2, G3,

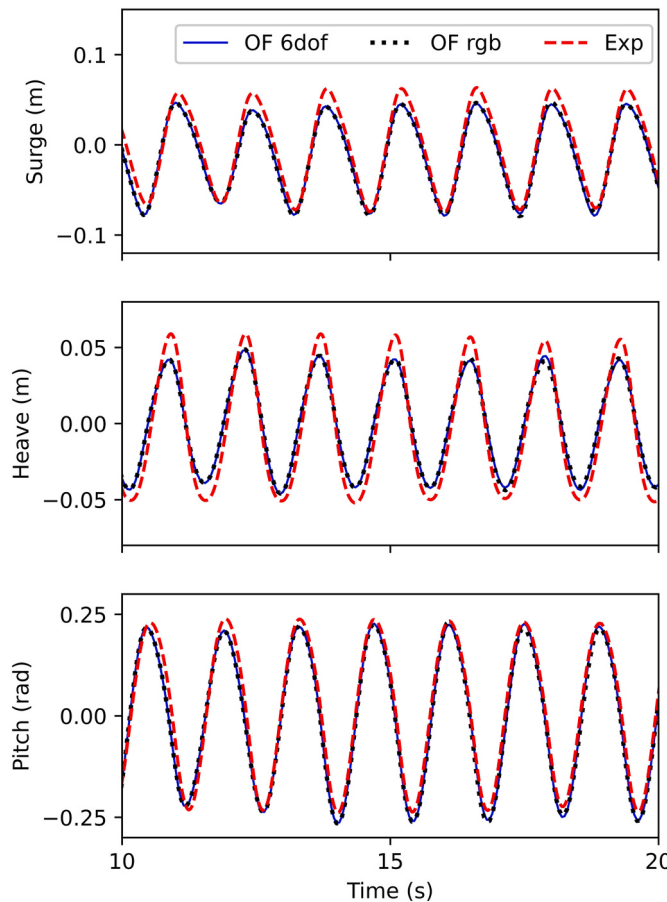


Fig. 4. Numerical and experimental results of the single FB motion.

and G4) are used to record the surface elevations. A global coordinate system $O\text{-}xyz$ is defined such that $x = 0$ is located at the center of the rectangular floating breakwater and $z = 0$ at the still water level. The draft of the breakwater is 0.16 m and the center of gravity is located at $z = -0.0948$ m. An active generating-absorbing wavemaker is applied to the inlet and outlet boundaries of the numerical wave flume (Higuera et al., 2013). Second-order wave theory is used to specify the velocities and VOF along the stationary inlet boundary. No slip condition is applied to the immovable bottom wall. The top boundary behaves like open atmosphere, which is defined by a combination of boundary conditions for pressure and velocity, permitting both outflow and inflow while maintaining stability. An empty condition is applied to the front and back walls. The overset grid technique is adopted to accommodate the body mesh movement. The boundary conditions for the overset patch are therefore all handled by the OpenFOAM's built-in overset library. At the wall boundaries, the pressure gradient is adjusted so that the boundary flux matches the velocity boundary condition.

Note that cell stretching is also applied to the rightmost 3 m of the flume to help damp the waves. The simulation is intended to run for up to 20 s and the time step is adjusted at runtime with a maximum Courant number limit of 0.5. The first-order implicit Euler scheme is used for time marching. The advective term is discretized using linear upwind scheme along with a linear interpolation scheme to calculate the gradient of the velocity. The diffusion term is discretized using the standard Gauss scheme in combination with a linear interpolation scheme for the diffusion coefficient and a corrected scheme for the surface normal gradient. The first advective term in the VOF equation is discretized using the vanLeer scheme and the second advective term using the linear scheme in order to produce smoother interfaces. A distance weighted interpolation scheme is used to exchange the flow

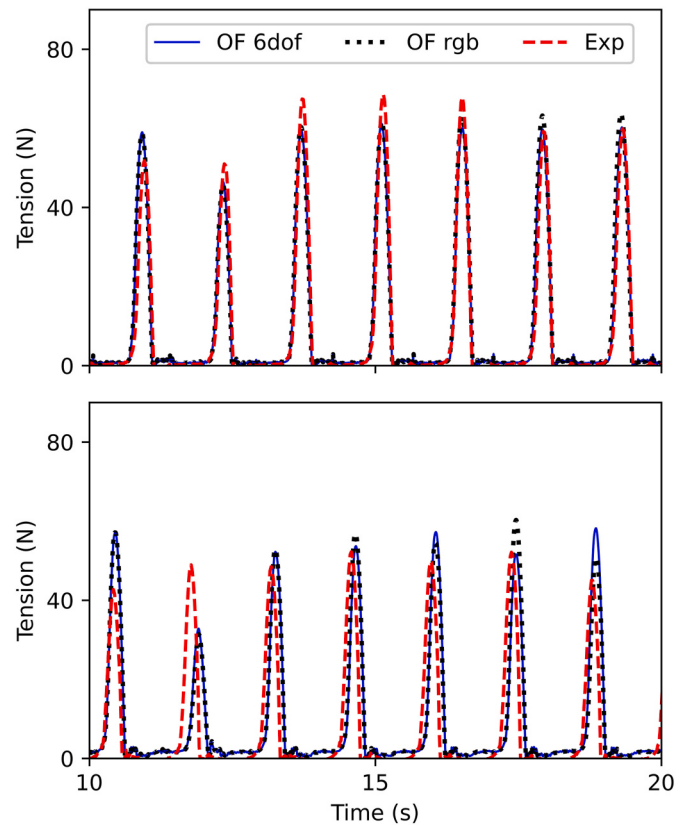


Fig. 5. Numerical and experimental results of mooring line tensions for the single FB test. Top: seaward line; bottom: leeward line.

information between the background mesh and the body-conforming overset grid. Other discretization schemes follow the standard practices of wave simulations using OpenFOAM's *interFoam* series of solvers (Chen and Hall, 2022). Both six-DoF motion and rigid body dynamics library are used to solve the breakwater motion. Only the MoorDyn mooring restraint is tested. For each time step, 3 outer correctors (PIMPLE iterations) are used along with two pressure correctors per PISO loop. Considering the oscillating nature of the pressure force (Gatin et al., 2017), a minimum of 3 outer correctors may be required to achieve a reasonable solution. To avoid numerical instabilities, the floating body acceleration is relaxed by a factor of 0.8. As a matter of fact, a factor of 1.0 does not lead to numerical instability for this case. The breakwater motions, surge in particular, increase marginally. A dynamic relaxation combined with certain convergence criteria may be adopted to speed up the convergence per time step (Dunbar et al., 2015). A novel algorithm was recently implemented obviating the need for outer iterations entirely (Roenby et al., 2024). According to the grid convergence study in Appendix A, it is sufficient to use a uniform grid size of 0.01 m to simulate this box-type floating breakwater. A non-uniform grid which is refined near the free surface and the breakwater is also found not to lose much accuracy while it can enhance the computing efficiency significantly.

3.1.2. Simulation results

Fig. 3 shows the comparison of the predicted surface elevation and the measured data for the single FB experiment. There is barely difference in the two sets of numerical results ('6dof' and 'rgb'). As the numerical simulation is conducted for 20 s only, surface elevation at the leeward wave gauges (G3 & G4) may not be fully established yet in the first several wave periods (10 s ~ 15 s). But later on, the wave shape changes and there appears better agreement between the numerical predictions and the experimental measurements. As a matter of fact,

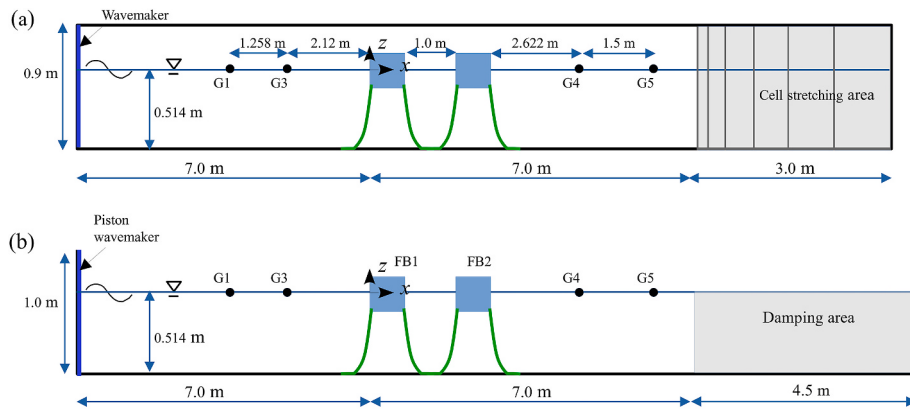


Fig. 6. Numerical model setup for the physical experiment of a twin floating breakwater (Chen et al., 2023). (a) OpenFOAM model setup; (b) DualSPHysics model setup.

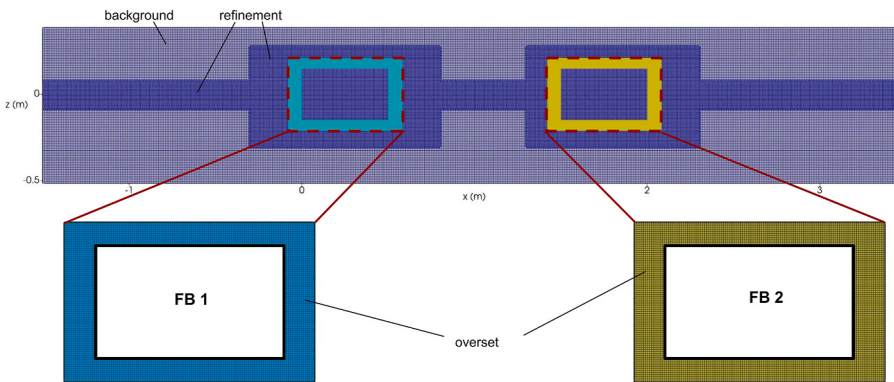


Fig. 7. Mesh setup in the vicinity of the twin floating breakwaters. Overset grids for the twin FBs overlay the background mesh.

there is excellent match in the first few waves experienced by the leeward wave gauges if we compare the numerical result with the first initial waves of the experimental data (not shown here). Overall, the numerical model is able to capture the wave shape changes, predicting better surface elevations at G1 & G2 than those at the leeward waves.

Figs. 4 and 5 show the comparison of numerical predictions and experimental measurements of the breakwater motion and the mooring line fairlead tension, respectively. Good agreements are achieved among the two sets of numerical results ('6dof' and 'rgb') and the experimental data. For some unknown reasons, the heave motion is consistently underestimated. While all the motions (surge, heave, and pitch) seem regular in time, the mooring tension exhibits slight irregularity due to some disturbances in both the numerical and the physical flume. The mooring code MoorDyn captures the sudden pick up and release of the tension in both mooring lines. The tension in the seaward line is in general larger than that in the leeward line.

3.2. A twin floating breakwater

3.2.1. OpenFOAM model setup

Fig. 6a shows the numerical model setup using OpenFOAM's two-phase flow solver. The 2D numerical flume is 17 m long and 0.9 m high. The still water level is fixed at 0.514 m. As in the physical experiments, four wave gauges (denoted G1, G3, G4 and G5) are used to record the surface elevations. Wave gauge G2 is not placed for relatively long waves. The two floating breakwaters, spaced 1 m apart, are identical in size and mass properties (Table 1). Each of the floating breakwaters is 0.745 m long, 0.5 m wide and 0.3 m high. The mass and moment of inertia are 55.875 kg and 2.20795 kg·m², respectively. Each breakwater is restrained by four identical stainless-steel mooring lines,

each having a total length of 0.62 m and an inserted spring with a stiffness of 2.6 N/mm. The upper end of the mooring line is connected to the bottom of the floating breakwater and the lower end is anchored to the flume bottom. The horizontal distance between the two attachment points is 0.358 m.

A global coordinate system O-xyz is defined such that $z = 0$ is located at the still water level and $x = 0$ at the seaward edge of the first floating breakwater. The draft of the floating breakwaters is 0.15 m and the center of gravity is located at $z = -0.0771$ m. The overset mesh is adopted to accommodate the body motion. Second-order wave theory is used to specify the velocities and VOF along the stationary inlet boundary. Both six-DoF motion and rigid body dynamics library are used to solve the breakwater motion. The boundary conditions, discretization schemes, and rigid body and mesh motion settings are the same as the single FB described above.

Although the OpenFOAM model is set up as a 2D simulation, a single cell with a width equal to 0.745 m is specified in the y-direction. Same as the physical experiments, four identical mooring lines are specified to restrain each of the twin rectangular FBs. Each mooring line is discretized into 10 equal segments. The normal and tangential drag coefficient are 2.4 and 0.05, respectively. No efforts are made to fine-tune these coefficients, as there are no measurements available for the mooring tensions. Three cases of regular waves are tested to validate the model, all having the same wave height 0.05 m but differing wave periods 1.4 s, 1.7 s, and 2.0 s.

The base grid size of the background mesh is 0.01 m, which is refined to 0.005 in the vicinity of the free surface and the breakwaters (see Fig. 7). The overset grid for the two floating breakwaters is uniformly 0.005 m. There are 10 grids per wave height and 518 grids per wave length for the shortest waves considered in this study. According to the

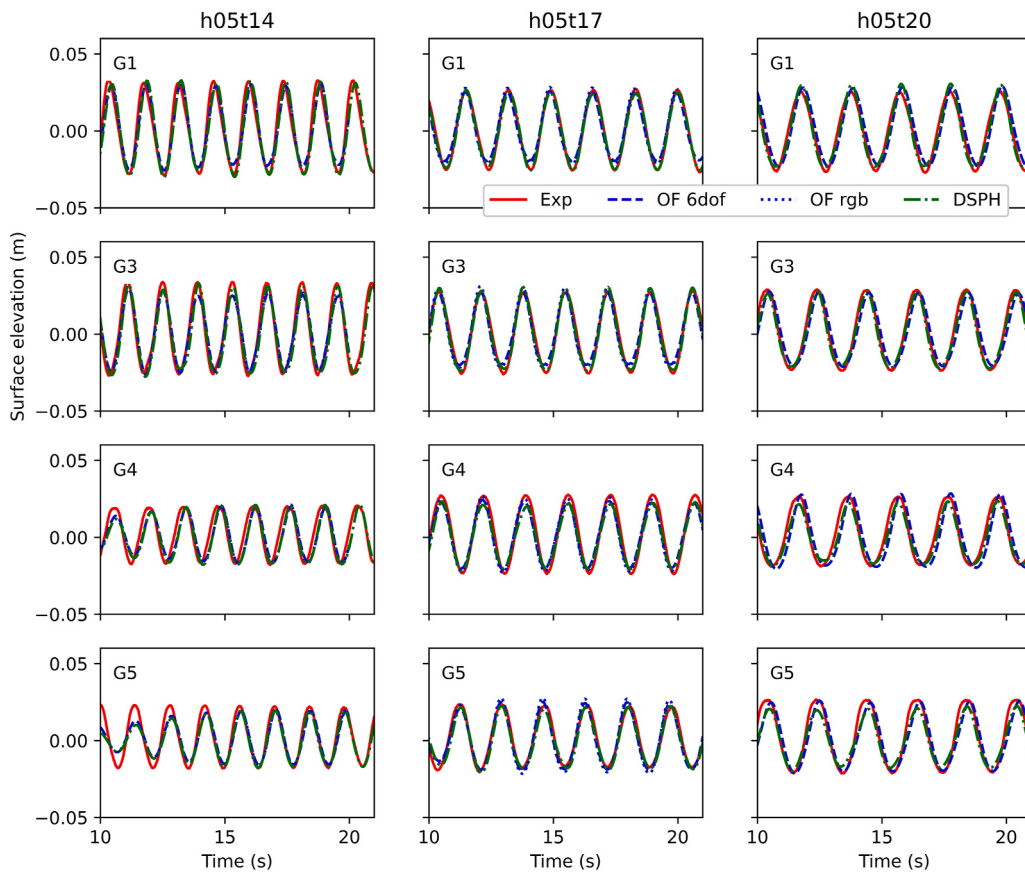


Fig. 8. Numerical and experimental results of surface elevations for the twin FB test in regular waves with height 0.05 m and periods 1.4 s (left), 1.7 s (middle), 2.0 s (right). Exp: experimental data (Chen et al., 2023); OF 6dof: OpenFOAM simulation using six-DoF motion library; OF rgb: OpenFOAM simulation using rigid body dynamics library; DSPH: DualSPHysics simulation.

convergence study in Appendix B, finer meshes may be required to achieve convergence for the surge motion. The heave and pitch motions are less sensitive to the grid size, and are deemed converged with a medium grid size of 0.005 m.

3.2.2. DualSPHysics model setup

Fig. 6b shows the DualSPHysics model setup, which uses the same coordinate system, wave gauges, and FB setup as its OpenFOAM counterpart. An active absorbing piston-type wavemaker is applied to the inlet, and the rightmost 4.5 m of the flume is designated as damping area for the transmitted waves (Altomare et al., 2017). Different from the OpenFOAM model setup which includes both air and water, the SPH model resolves only the water phase. The wavemaker at inlet, the two FBs, and the flume bottom and outlet are all resolved as moving/non-moving boundary particles.

To simulate the twin FB in a 2D setup, the FB length is scaled up from 0.745 m to 1.0 m. The same is done with FB mass, moment of inertia, and mooring spring stiffness (He et al., 2023). Two mooring lines, each equivalent to two lines used in the physical test and OpenFOAM model, are used to restrain each of the FB's motion. The mooring lines are solved by MoorDyn + library, which is adapted from MoorDyn to couple specifically with the SPH flow solver (Domínguez et al., 2019). The DualSPHysics simulation is run using Tesla K40m GPU at UNM's Xena cluster, which has 2880 CUDA cores and a computing capacity of 3.5. According to the convergence study in Appendix B, the particle size is chosen to be uniformly 0.006 m (multi-resolution is not yet supported).

3.2.3. Simulation results

Fig. 8 presents numerical and experimental surface elevations for the twin FB tests in regular waves with height 0.05 m and periods 1.4 s, 1.7

s, and 2.0 s. Negligible discrepancies are seen between the two sets of OpenFOAM simulations using six-DoF ('OF 6dof') motion library and rigid body dynamics ('OF rgb') library. The only noticeable difference appears at wave gauge G5 for case h05t17. There are overall good agreements between the numerical results and the experimental data for all the three cases. The same can also be said for the DualSPHysics simulation, except that the SPH model underestimates the surface elevation of the transmitted waves for case h05t20.

Figs. 9–11 show the comparison of numerical and experimental results of breakwater motions for the twin FB tests in regular waves for cases h05t14, h05t17, and h05t20, respectively. There are overall good agreements between OpenFOAM and DualSPHysics simulation results and the measurements for the latter two cases (Figs. 10 and 11). There are significant discrepancies in surge motion of case h05t14; the experimental data show that both FBs have drifted about 0.1m down-wave from their initial equilibrium positions (Fig. 9). The OpenFOAM results momentarily catches up the surge motion of FB1 and nearly catches up that of FB2. The DualSPHysics results, however, never obtain the experimental drifts of both FBs. Instead, it is observed that both FBs' surge motions oscillate steadily around an equilibrium position not far from their initial positions. The DualSPHysics model employs a piston-type wavemaker to generate the waves. Both 1st order and 2nd order wave theories are tested, and no improvement is observed for the surge predictions. The same is true for the relaxation zone technique, which, instead of mimicking a physical wavemaker, specifies a transition region to smoothly generate the targeted waves. The unsatisfactory prediction of surge motion may arise from probable differences in the present 2D model setup and the physical wave flume; in the latter case, a narrow gap was placed between the breakwater and the flume side walls. While allowing for the breakwater motion without friction against the flume

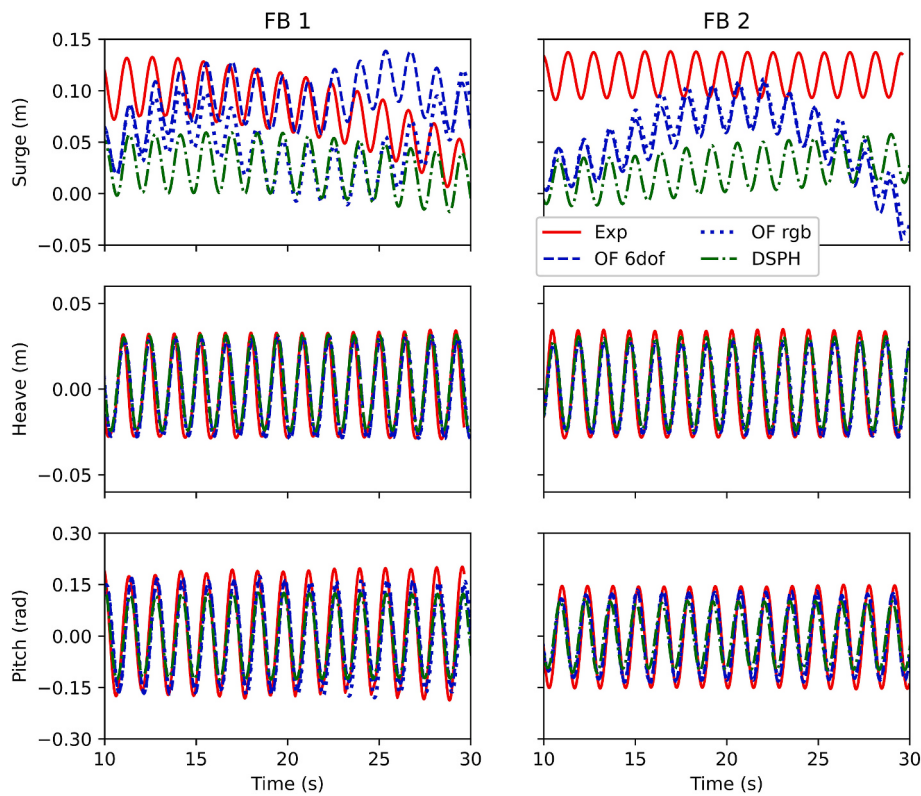


Fig. 9. Numerical and experimental results of breakwater motions for the twin FB test h05t14 (wave height 0.05 m and period 1.4 s). Refer to Fig. 8 for legend clarifications.

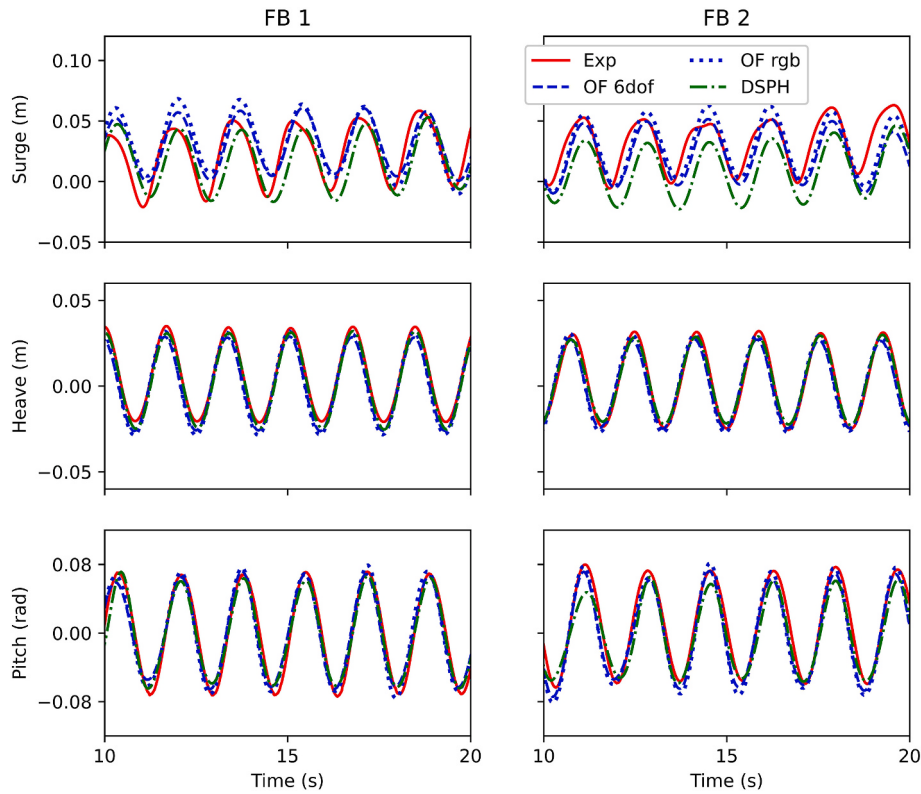


Fig. 10. Numerical and experimental results of breakwater motions for the twin FB test h05t17 (wave height 0.05 m and period 1.7 s).

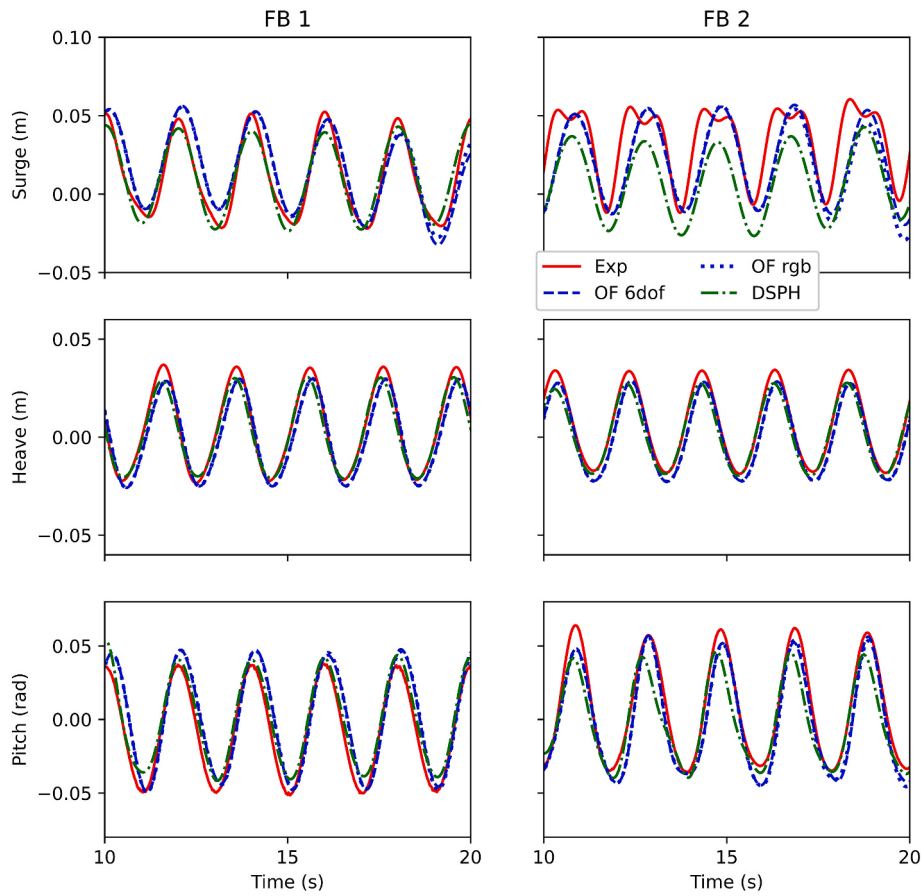


Fig. 11. Numerical and experimental results of breakwater motions for the twin FB test h05t20 (wave height 0.05 m and period 2.0 s).

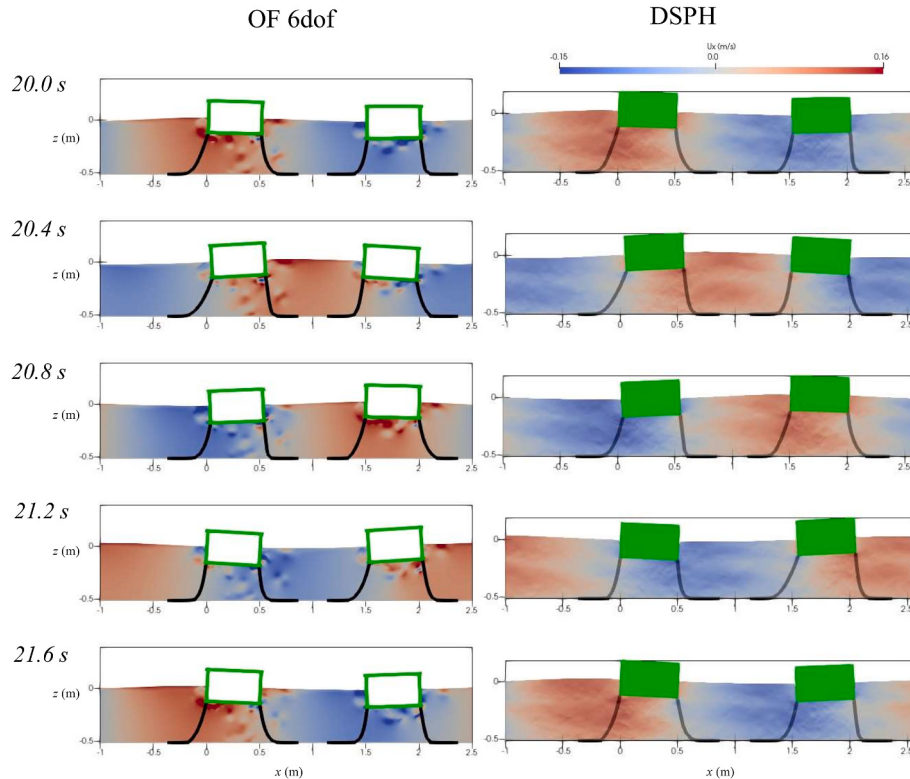
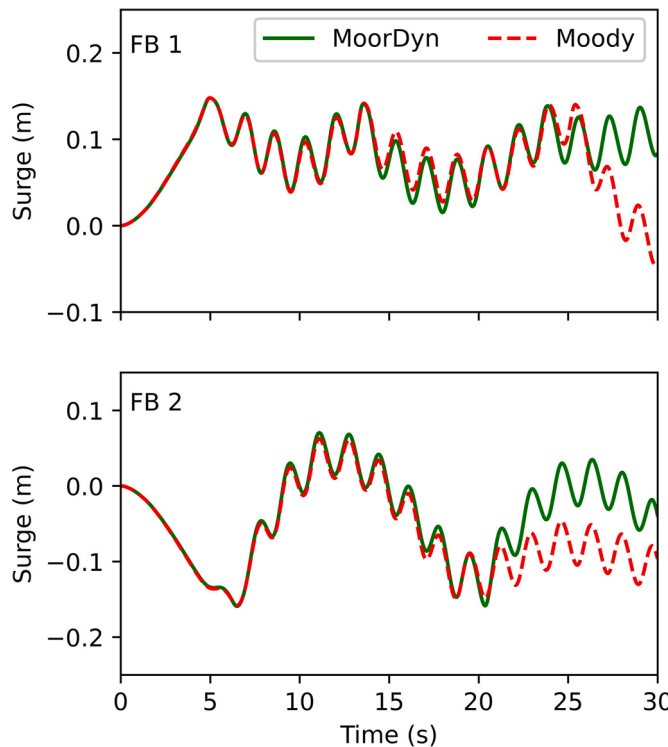


Fig. 12. Comparison of instantaneous horizontal velocity contours and mooring configurations predicted by OpenFOAM (OF 6dof) and DualSPHysics (DSPH) for case h05t17.

Table 2

Comparison of CFD simulation runtime by OpenFOAM and DualSPHysics.

Parameters	OpenFOAM	DualSPHysics
Operating system	Rocky Linux	CentOS 7
Computing resources	64 CPUs Intel Xeon Gold 6242 @ 2.80 GHz Intel Xeon Gold 6226R @ 2.90 GHz	1 Nvidia Tesla K40m GPU Intel Xeon CPU E5-2640 @ 2.60 GHz
Grid/particle size	5 mm	6 mm
Total grids/particles	236k	533k
Physical time	22 s	19.4 s
Runtime	6.6 h	48 h
Runtime per physical second	18 min	148 min

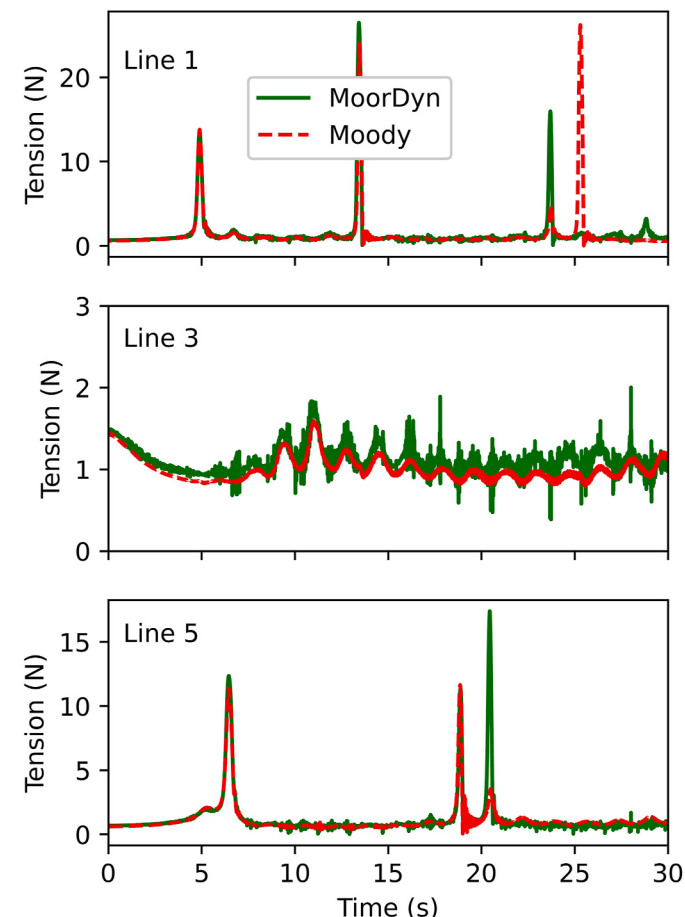
**Fig. 13.** Surge motion of a twin FB with shared mooring lines in regular waves (h05t17).

walls, this gap may cause slight wave diffraction and undesirable motions, thus affecting the waves forces on the breakwater and the motion measurements (Chen et al., 2023). The wave diffraction and undesirable motions are supposed to be more pronounced for short waves than for long waves. This may partly explain why the numerical models predict better breakwater motions in relatively long waves (Figs. 10 and 11). The single FB test in Section 3.1 seems not to suffer much from this issue, although the crest amplitude of the surge response is indeed underpredicted (Fig. 4). These discrepancies in surge predictions were also noticed by Palm et al. (2016). For waves with the same height, their Fig. 8 demonstrated larger discrepancies for short waves than for long waves. It is worth noticing that the motion predictions by the six-DoF solver (OF 6dof) and the multibody dynamics solver (OF rgb) deviate at some point in time from each other. These discrepancies seem to be more pronounced for short waves than for long waves (Fig. 9 versus Fig. 11). The largest discrepancy occurs in the surge motion predictions of FB 1 for case h05t14 (Fig. 9), while the surge motion predictions of FB 2 by the two solvers largely coincide with each other. At the time of writing, no definite reasons could be found to explain the differences.

The OpenFOAM and DualSPHysics results are in phase with each other. But they have inexplicable phase shift relative to the surge measurements of FB2 for case h05t14 (Fig. 9). Certain time shift may

have accidentally occurred with the recordings. For cases h05t17 and h05t20, both numerical results generally follow the patterns of the measured surge motion, albeit with some small discrepancies in the oscillation positions and amplitudes. The best comparisons between the numerical and experimental results are achieved for the heave motion, which are dominated by the hydrostatic restoring stiffness. There are also satisfactory agreements for the pitch motions. While the OpenFOAM results match slightly better with the measurements, the SPH results underestimate the pitch motions of both FBs for case h05t14 and of FB2 for case h05t20.

Fig. 12 shows the comparison of instantaneous horizontal velocity contours and mooring system states obtained by OpenFOAM and DualSPHysics for case h05t17. The OpenFOAM model is a two-phase flow solver, encompassing both the water and the air (clipped to show the water wave motion only). The DualSPHysics model resolves only the water phase. The top boundary of the computational domain is bound by

**Fig. 14.** Mooring line tensions of a twin FB with shared mooring lines in regular waves (h05t17).

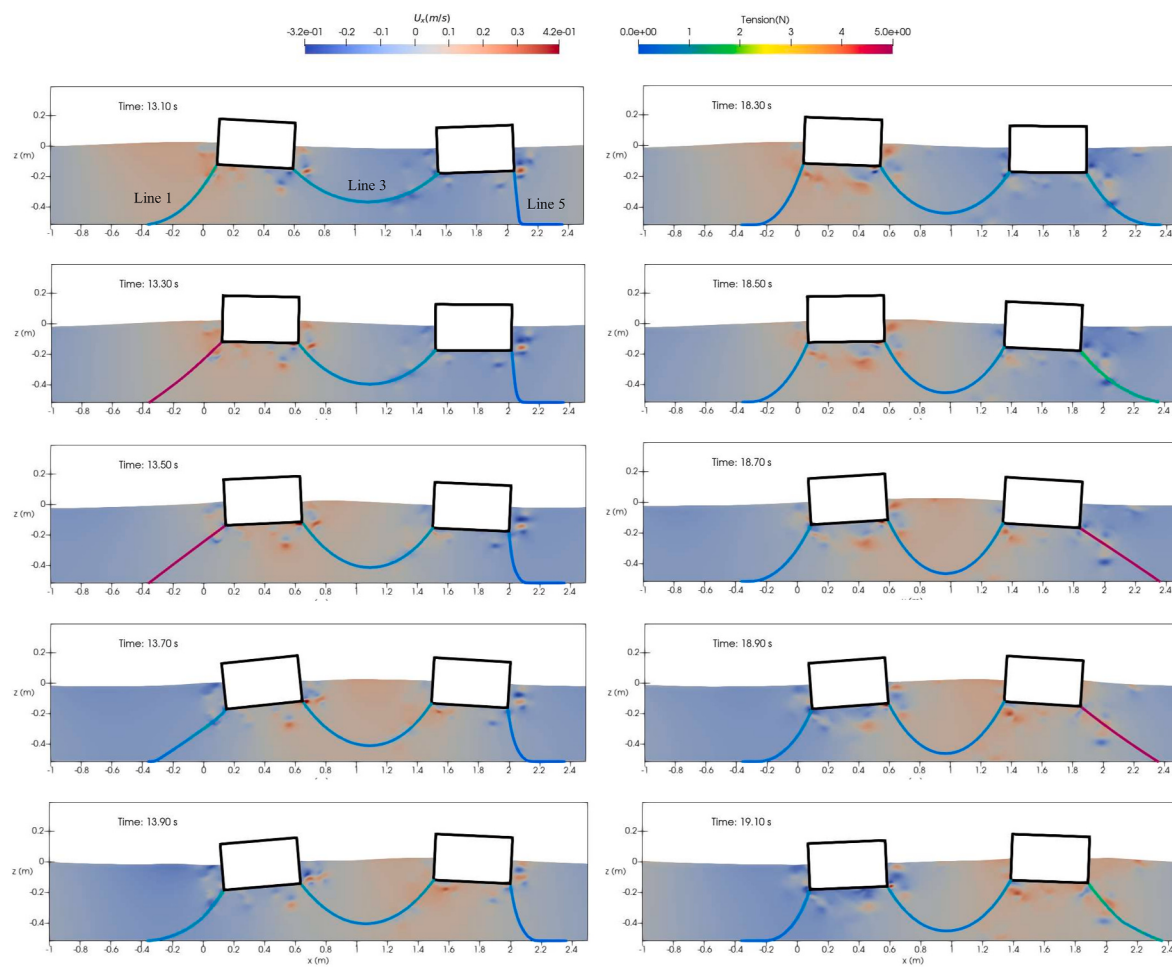


Fig. 15. Snapshots of instantaneous horizontal velocity contours and mooring configurations of a twin FB with shared moorings in regular waves (h05t17).

the free surface and the two FBs. Despite the difference in the domain setup, the two models actually have about the same number of computational cells/particles, 236k cells for the OpenFOAM model and 264k particles for the DualSPHysics model.

Table 2 lists the computing resources and simulation wall-clock time for case h05t17. It should be noted that the DualSPHysics model solves the mooring dynamics only once per time step, while the OpenFOAM model performs three iterations per time step in order to better converge

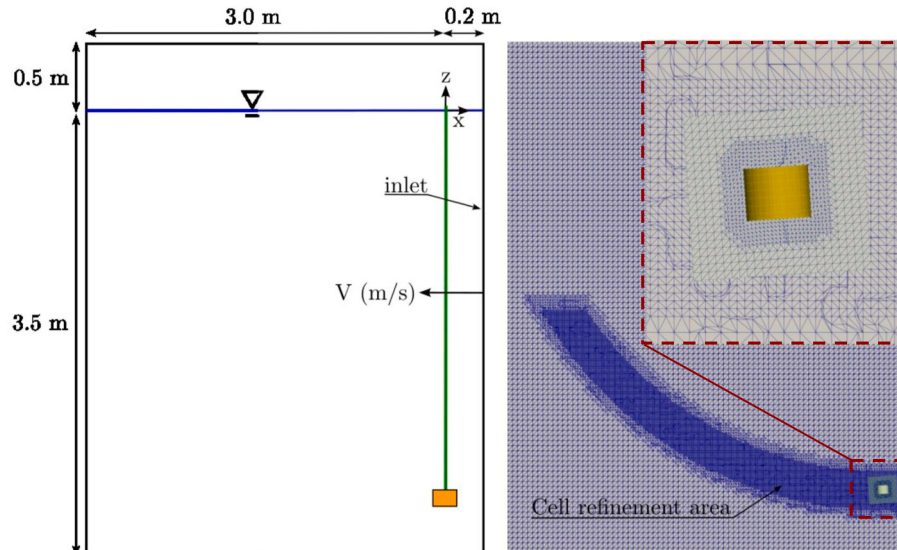


Fig. 16. Numerical model setup for the physical experiment of a towed subsurface object (Guan et al., 2021). Left: domain dimensions. Right: background mesh and overset grid.

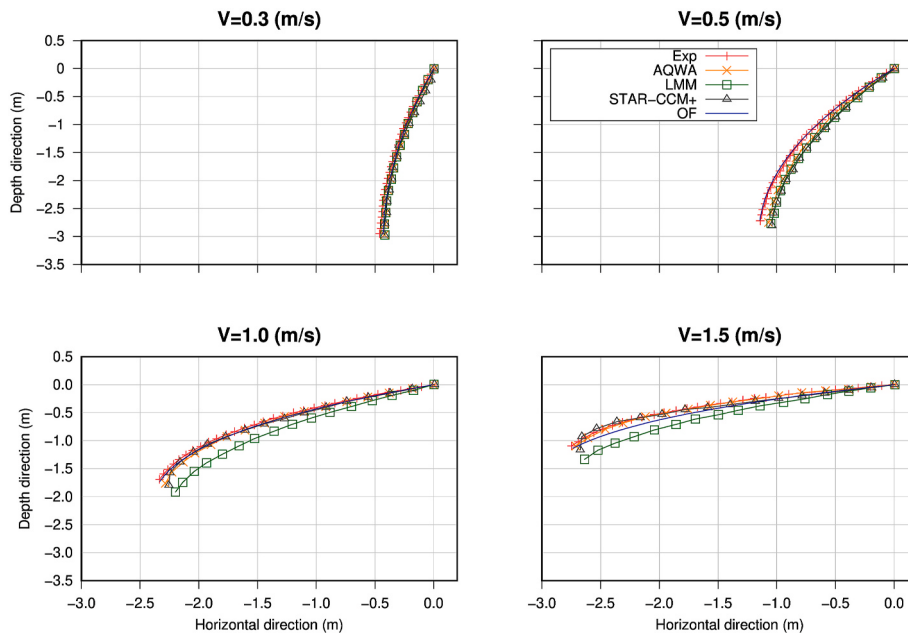


Fig. 17. Numerical and experimental results of the towing cable posture with four towing speeds.

both the motion and mooring response. It is observed that the OpenFOAM runtime (using six-DoF motion library) is in general noticeably longer for short waves than for long waves, while the DualSPHysics runtime for different cases are about the same. For the same number of cells/particles, the OpenFOAM model runs significantly slower than the DualSPHysics model, for the fine grids/particles in particular. While the former may increase the number of CPUs used to hundreds, these computing units, however, are not generally available on a typical HPC cluster. Each cluster may have specific policies limiting the number of CPUs accessible to each user and the maximum wall-time allowed for each job. In comparison, a single GPU, such as the Nvidia Tesla K40m used in this study, is more readily available. It is logical to speculate that a high-end GPU with higher computing capability may further increase the computational efficiency. In this perspective, the DualSPHysics model is an attractive alternative to mesh-based CFD models, which can significantly speed up the runtime required for common engineering simulations.

To demonstrate the OpenFOAM model's capability to simulate floating structures with shared moorings, the mooring system of the twin FB (8 mooring lines in total, Fig. 6) is revised so that the twin FB is interconnected with two shared mooring lines, each of which is 1.06 m long. There are now a total number of 6 mooring lines restraining the floating bodies' motion. All lines share the same properties as in the individually moored system. Figs. 13 and 14 show the time history of the surge motion and mooring line tensions for this twin FB with shared mooring lines in regular waves (h05t17), predicted by a coupled OpenFOAM (rgb) and mooring model. It is clearly observed that the surge motions of FB1 and FB2 are tightly coupled, with the wave frequency surge component superimposed with a relatively long cycle of

second-order drift. Correspondingly, the mooring tensions exhibit large spikes whenever the external mooring lines (lines 1 & 5, see the first panel plot in Fig. 15) reach the positive/negative extremities of the surge displacements. The shared mooring line (line 3) experiences only mild tension in this case, as its length is sufficiently long to accommodate the relative surge motion while still maintaining a catenary shape throughout the simulation. A shorter length of 1.02 m is observed to cause straightening of the shared line and thus tension spikes as seen in the external lines.

Fig. 15 presents the instantaneous horizontal velocity contours and mooring configurations predicted by the coupled OpenFOAM and mooring model (Moody). The left column corresponds to instants, 13.1 s–13.9 s, when the windward lines (line 1) of twin FB experience snap loads. The right column corresponds to instants, 18.3 s–19.1 s, when the leeward lines (line 5) experience snap loads. To avoid these costly tension spikes, it is advisable to carefully configure the shared mooring system with intermediate weights/floats in order to decouple the body motions and the extreme mooring tensions.

3.3. A towed subsurface object

3.3.1. Numerical model setup

A typical underwater towing system consists of a tugboat towing a floating buoy, which is in turn connected to a subsurface object through a towing cable. The steady-state position and posture of a simple towed system consisting of a subsurface cylinder and a towing cable (Guan et al., 2021) are simulated using the coupled OpenFOAM-mooring model. The subsurface cylinder has a diameter of 8.4 cm and a height of 6.6 cm. The gravity of the object is 9.95 N, and the buoyancy is 3.43 N. The towing cable is made of nylon, which is 3 m long, 1 cm in diameter, and 1050 kg/m³ in density. The positions and postures of the towing cable at four towing speeds of 0.3 m/s, 0.5 m/s, 1.0 m/s, and 1.5 m/s are studied.

The computational fluid domain contains 1.6 million cells in a rectangular box defined by the dimensions $-3.0 \leq x \leq 0.2$ m, $-0.3 \leq y \leq 0.3$ m and $-3.5 \leq z \leq 0.5$ m. A global coordinate system, O-xyz, is established, with the origin $x = 0$ and $y = 0$ located at the center of the subsurface object, and $z = 0$ at the still water level. The top end of the towing cable is held stationary, which is located 0.03 m above the still water level. The lower end of the towing cable is set at $(0, 0, -2.97)$ m.

Table 3

Results of towing cable tip positions and deviations with experimental data (Guan et al., 2021).

Current (m/s)	OpenFOAM simulation		Experimental data		Deviation	
	X _{OF} (m)	Z _{OF} (m)	X _{Exp} (m)	Z _{Exp} (m)	D _x (%)	D _z (%)
0.3	-0.431	-2.940	-0.460	-2.950	6.30	0.34
0.5	-1.145	-2.701	-1.141	-2.720	0.35	0.70
1.0	-2.333	-1.713	-2.336	-1.691	0.13	1.30
1.5	-2.736	-1.117	-2.748	-1.093	0.44	2.20

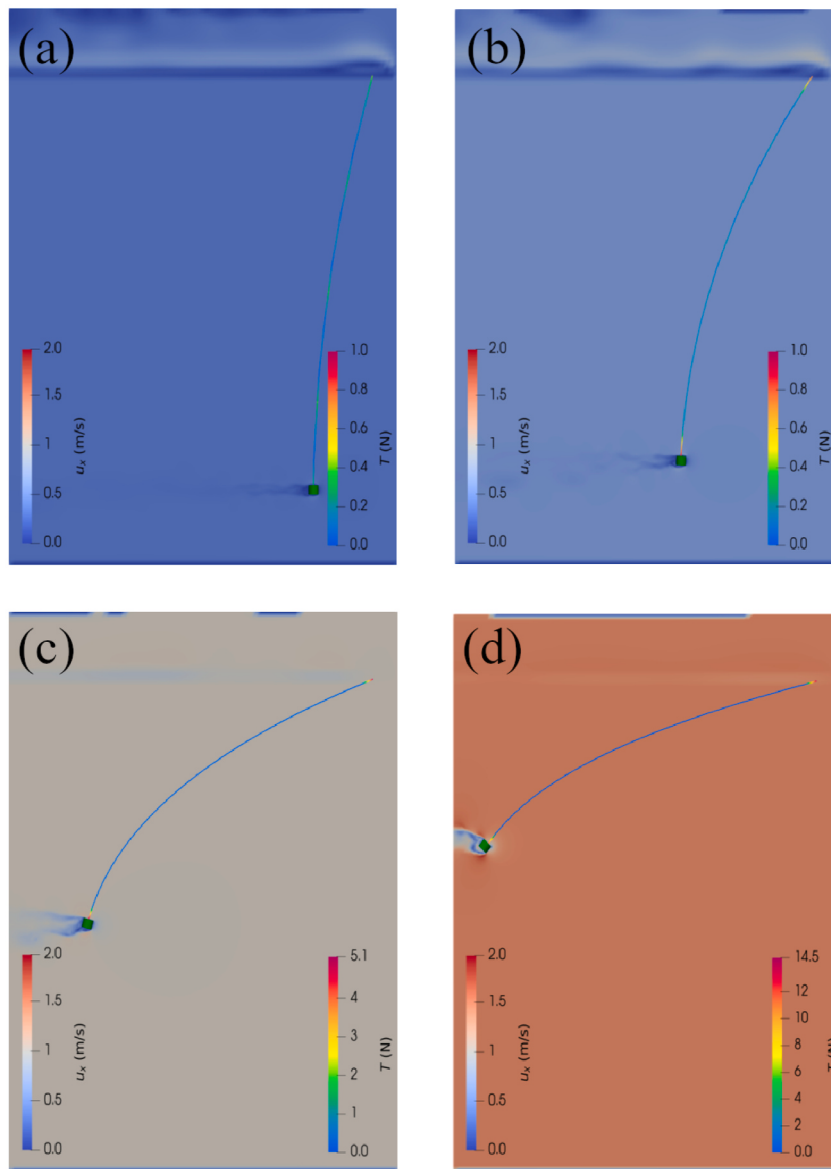


Fig. 18. Snapshots of instantaneous horizontal velocity contours and towing cable posture and tension predicted by OpenFOAM for a towing speed of (a) 0.3, (b) 0.5, (c) 1.0, and (d) 1.5 m/s.

The initial center of gravity of the heavy object is thus positioned at (0, 0, -3.003) m. Instead of mimicking the towing operation, a background current is imposed. The six-DoF dynamic library is used to solve for the motion of the subsurface object, although the rigid body dynamics library is equally applicable. The overset mesh approach is adopted to facilitate the large-scale body motion.

Fig. 16 illustrates the OpenFOAM model setup for the towed subsurface object experiment (Guan et al., 2021), including views of the background mesh and the overset mesh. The base grid size of the background mesh is 0.0283 m, which is refined to 0.0071 m along the body's prospective trajectory. The overset grid for the subsurface object is maintained at a uniform size of 0.0071 m. This size selection ensures that there is a minimum of 10 cells placed between the body patches and the overset patch. Additionally, the mesh is subject to refinement near the body's wall to enhance the representation of the structure and capture the flow patterns in the immediate vicinity. Grid convergence study has been conducted to confirm the cell sizes selection. The towing cable is discretized into 60 equal length segments. The normal and tangential drag coefficients of the towing cable are set as 1.2 and 0.025, respectively. The simulations are expected to run for a maximum of 20 s,

with the time step adjusted at runtime to maintain a maximum Courant number of 0.9. Body acceleration is relaxed by 0.4 at each time step, for which only one outer correction is performed.

3.3.2. Simulation results

Fig. 17 shows the comparison of OpenFOAM results of the steady-state posture of the towing cable with experimental measurements (Guan et al., 2021) and numerical simulations obtained by AQWA, Lumped-Mass Method (LMM), and STAR-CCM+ (Yang et al., 2022). There are no significant differences between the OpenFOAM simulations ('OF') and the experimental measurements. It is worth noting that at a towing speed of $V = 0.5$ m/s, while there is generally good agreement in the posture predicted by OpenFOAM, the other numerical methods (AQWA, LMM, and STAR-CCM+) present significant differences. At a towing speed of $V = 1.0$ m/s and $V = 1.5$ m/s, the results of the LMM method differ significantly from those of OF, AQWA, and STAR-CCM+. It is in the case of $V = 1.5$ m/s where OpenFOAM exhibits more noticeable differences from the experimental data for the lower-middle section of the towing cable. However, the tip position of the towing cable shows negligible difference from the experimental data.

Table 3 lists the results of the submerged body's coupling position with the towing cable and deviations with experimental results (Guan et al., 2021). The largest deviation occurs at a towing speed of 0.3 m/s (6.3%) for the horizontal component and at a towing speed of 1.5 m/s (2.2%) for the vertical component. Fig. 18 shows the simulation snapshots of horizontal velocity contours and towing cable tension values at steady-state (20 s) predicted by the coupled OpenFOAM and MoorDyn model. The posture of the subsurface object and the towing cable change significantly with the increase of towing speeds. It should be noted that a single (subsurface) body is simulated for this case study. Using the mooring restraints developed for the *rigidBodyMotion* library, it is straightforward to accommodate a second (surface) floating body to simulate a complete underwater system towing in still waters or waves.

4. Concluding remarks

To help analyze multiple floating structures operating in close vicinity in the coastal and ocean environments, this paper presents the development and validation of a high-fidelity coupled CFD-mooring model to simulate the dynamic response of these structures using the leading open-source CFD toolbox, OpenFOAM. The two rigid body motion libraries that solve body motions by Newton's second law and articulated body algorithm, respectively, are extended with an open-access mooring restraint library, *foamMooring*. The new library serves as an interface between OpenFOAM's rigid body motion solvers and three mooring analysis codes, namely, a quasi-static mooring model MAP++, a lumped-mass mooring model MoorDyn, and a finite element model Moody. Thanks to recent developments of MoorDyn, the coupled CFD-mooring model using the built-in *sixDoFRigidBodyMotion* library can now be applied to simulate multiple individually moored bodies. Because of its inherent multibody dynamics formulation, the *rigidBodyMotion* library is more capable; it is particularly suited to simulations of multiple structures interconnected via hinges or shared moorings. The coupled CFD-mooring model is validated against experimental measurements for a single box-type floating breakwater and a twin floating breakwater moored in regular waves. The overset grid method is adopted to solve the mesh motions of (multiple) rigid bodies. The coupled model is also verified by comparing results from the two rigid body motion solvers in OpenFOAM and a meshless SPH solver DualSPHysics. Overall, good agreements are achieved for the heave and pitch motions, as well the surge motion in relatively long waves. However, for the twin floating breakwater tests in short waves, it was found that both OpenFOAM and DualSPHysics models may have difficulty in predicting the surge response accurately. These 2D numerical flumes may not be an exact replica of the physical wave flume, in which a narrow gap was placed between the breakwater and the flume side walls. While allowing for the breakwater motion, this gap may cause slight wave diffraction and undesirable motions, thus affecting the waves forces on the breakwater and the motion measurements (Chen et al., 2023).

Results from the three mooring models (Appendix C) are comparable for the mild wave cases studied in the paper. Numerical instability may arise when applying these mooring models to simulate laboratory-scale physical tests. Because of its open-access, MoorDyn affords users more freedom in controlling the mooring system output and generating

visualization files at runtime. The coupled CFD-mooring model has also been validated using experimental measurements for a subsurface object with towing cables. In general, it demonstrates good agreement in terms of the position and posture of the towing cable across four different towing speeds. Using the mooring restraints developed for the multi-body dynamics library, the applicability of the model can be extended by incorporating the dynamics of a floating surface object towing in the presence of waves.

Three-dimensional CFD simulations of multiple floating structures can be computationally intensive. But the development of coupled potential flow and viscous flow solvers makes it computationally amenable to conduct high-fidelity simulations of multiple (interconnected) structures in a relatively large 3D domain (Aliyar et al., 2022; Lu et al., 2022). The open-access mooring restraints library developed in this work can be compiled as a dynamic library and loaded at runtime into such coupled flow solvers. Apart from the floating array of wind and wave farms, it is straightforward to apply the coupled CFD-mooring model to study gap resonance and vessel stability which respectively occur during offloading and lifting/installation operations. Using the articulated body algorithm, it can also be applied to other floating structure systems, such as floating treatment islands, floating solar farms, open ocean aquaculture farms, and towed-body system dynamics.

CRediT authorship contribution statement

Haifei Chen: Writing – review & editing, Writing – original draft, Visualization, Validation, Software, Methodology, Investigation, Formal analysis, Conceptualization. **Tanausú Almeida Medina:** Writing – review & editing, Writing – original draft, Visualization, Validation, Investigation. **Jose Luis Cercos-Pita:** Writing – review & editing, Writing – original draft, Validation, Software, Methodology.

Declaration of competing interest

The authors declare that they have no known competing financial interests or personal relationships that could have appeared to influence the work reported in this paper.

Data availability

The code is available at <https://gitlab.com/hfchen20/foamMooring>

Acknowledgement

The authors would like to thank the UNM Center for Advanced Research Computing (CARC), supported in part by the National Science Foundation, and Centro de Supercomputación de Galicia (CESGA) for providing the computing resources used in this work. Part of this research work was made possible through the financial support provided by Universidade da Coruña, Campus Industrial de Ferrol (Galicia, Spain) and Coremarine Solutions SL (Madrid, Spain). The authors would also like to thank Mr. Lois Veiga for proofreading the manuscript and Dr. Yong Liu for providing the experimental data of the floating breakwaters. The mooring restraints package developed in this work can be accessed at <https://gitlab.com/hfchen20/foamMooring>.

Appendix A. Grid convergence study for the single FB test

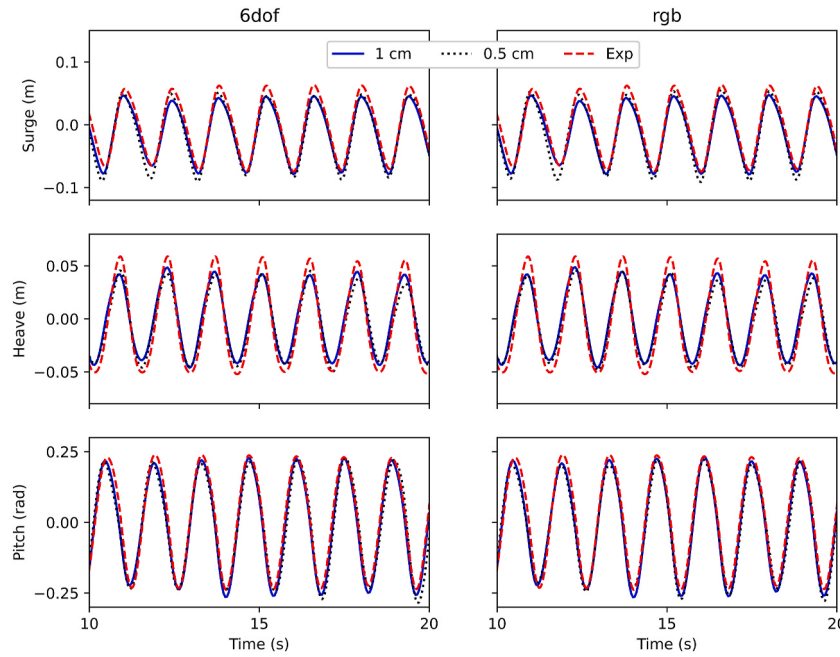


Fig. A.1. Single FB motion predictions by two grids using OpenFOAM coupled with MoorDyn. Left column: six-DoF motion library; right column: rigid body dynamics library.

Grid convergence tests for the single FB were conducted using both six-DoF motion and rigid body dynamics library in OpenFOAM. All runs were performed using 32 CPUs on UNM's CARC Hopper cluster. Fig. A1 shows the breakwater motions predicted by two grids using the MoorDyn mooring restraint. Apart from the slight difference in the surge predictions by the two grids, the heave and pitch motions clearly converged. The medium grid size of 1 cm is the same in both x - and z -directions and uniform across the entire computational domain. The total number of background and overset mesh cells is 95.8k. The wall-clock time for a 20 s simulation is about 0.9 h for one outer corrector per time step, and 1.6 h for three outer correctors per time step. It was found that solving the mooring system and thus the body motion only once per time step resulted in slightly larger tension in the mooring lines. The motion predictions were largely unaffected though, because of the mild wave condition in this test case. After all, at the beginning of each time step, the mooring system is solved using the body's motion information from the previous time step. If there is only one outer iteration per time step, the mooring tension predicted is obviously incompatible with the body motion state. For more accurate tension predictions (motion as well), more than one outer iteration may be necessary, which ensures a tighter coupling between the fluid motion and the rigid body motion in each time step. Thus, three outer correctors are used for results presented in this paper. A uniformly fine grid of 0.5 cm across the entire computational domain was used for six-DoF motion simulation, resulting in about 383k cells. The wall-clock time for a 20 s simulation using 32 CPUs is about 32.5 h. For rigid body dynamics simulation, a base grid size of 1 cm was refined only in the vicinity of free surface and the breakwater (see Fig. 7 for a demonstration of such a non-uniform mesh), generating about 175k cells. It took about 21.9 h to complete a 20 s physical time simulation.

Appendix B. Grid convergence study for the twin FB test

Grid convergence test was conducted to determine the cell size for the twin FB simulations using OpenFOAM. Three grids with minimum cell sizes of 1 cm, 5 mm, and 2.5 mm were used to simulate case h05t17 using the 6dof motion library, resulting in a total number of 133k, 236k, 533k cells, respectively. The wall-clock time for a 22 s run using 64 CPUs on UNM's Hopper cluster was about 1.9 h for the coarse grid and 6.6 h for the medium grid. The runtime for the fine grid was terminated at 19.4 s when it reached the resource time limit of 48 h. Fig. B1 shows that coarse grid tends to underestimate the heave motion. Clear convergence was obtained between the heave/pitch motions predicted by the medium and fine grids. However, it seems more difficult to achieve convergence for the surge motion. The predicted surges by the medium and fine grids are initially the same but later on they tend to deviate slightly as the simulation progresses.

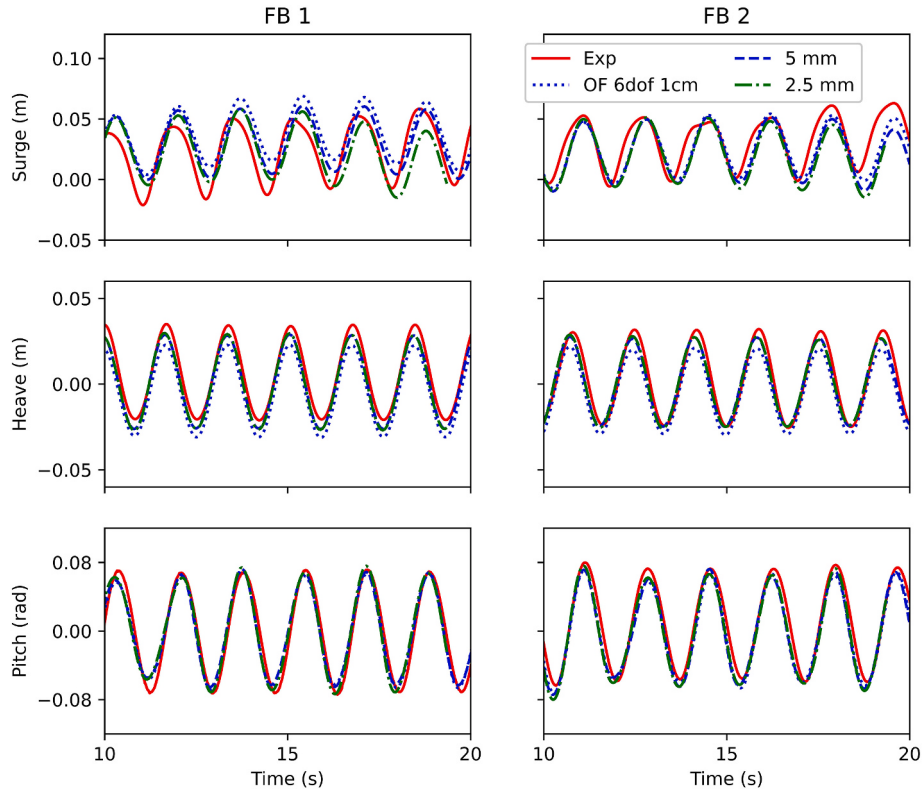


Fig. B.1. Breakwater motion predictions for the twin FB test using OpenFOAM with three grid resolutions (wave height 0.05 m and period 1.7 s).

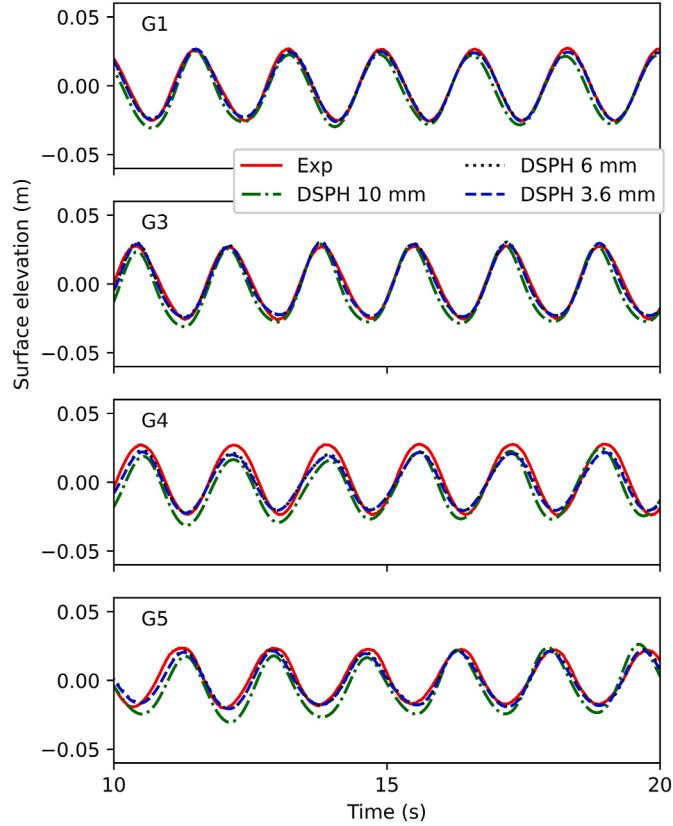


Fig. B.2. Surface elevation predictions for the twin FB test using DualSPHysics with three particle resolutions (h05t17: wave height 0.05 m and period 1.7 s).

Grid convergence test was also conducted to determine the particle size using DualSPHysics. Uniform size particles were generated across the computational domain. A particle size of 10 mm, 6 mm, and 3.6 mm resulted in a total of about 94k, 264k, and 731k particles, including both the fluid

and the boundary (fixed/moving/floating) particles. The wall-clock time for a 30 s run on UNM's Xena cluster was about 0.8 h, 2.4 h, and 9.6 h, respectively. It was observed that particle size 10 mm is not fine enough to capture the transmitted waves (G4 & G5 in Fig. B2) leeward of the second FB and converge the surge motions of both FBs (Fig. B3). There are virtually no differences between the surface elevation and heave/pitch motions predicted by the two finer particle sizes (6 mm and 3.6 mm). It is more difficult to achieve convergence for the surge motion of the second FB, in particular. The same observations were true for case h05t14.

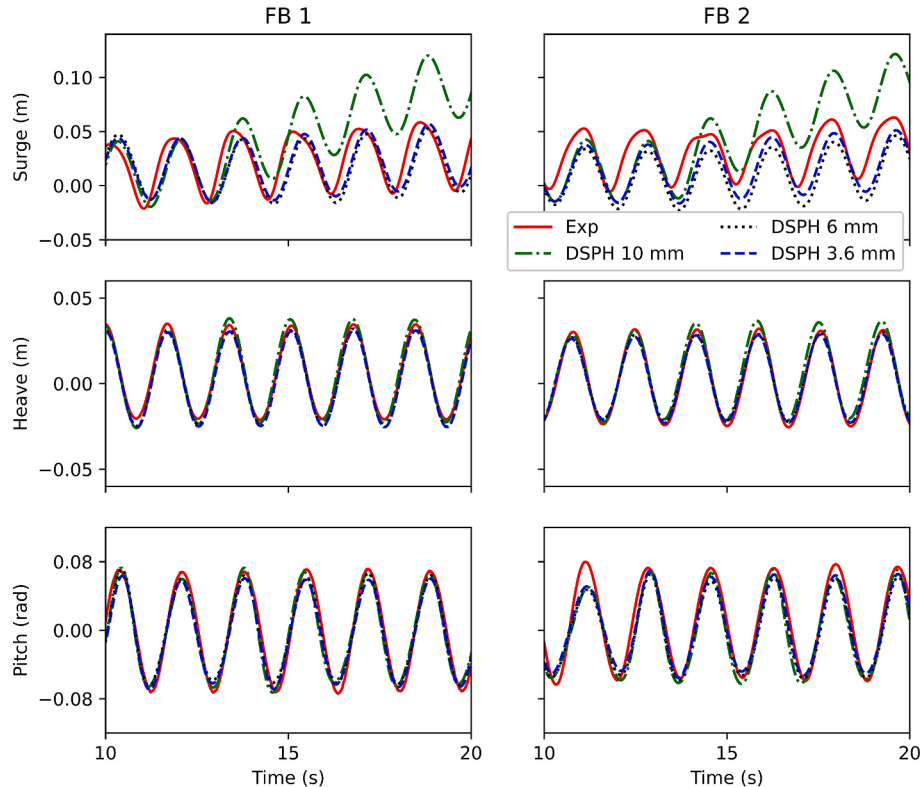


Fig. B.3. Breakwater motion predictions for the twin FB test using DualSPHysics with three particle resolutions (wave height 0.05 m and period 1.7 s).

Appendix C. Comparison of twin FB motion predictions by different mooring codes

Fig. C1-C.3 show the comparison of breakwater motion predictions by three mooring codes MAP++, MoorDyn, and Moody for the twin FB test using OpenFOAM's rigid body dynamics library. There were virtually no differences between the heave and pitch motions among the predictions by three mooring codes. The only noticeable difference was observed for the surge motion. The shorter the waves, the larger the discrepancy. For case h05t14, both breakwaters experience large pitch motions, which makes the mooring system highly dynamic. Both MAP++ and MoorDyn were able to simulate this case, while Moody failed to converge at around 11.8 s. Specifically, the mooring lines in leeward of FB 1 returned *nan*, which in turn crashed the simulation. There are large differences in the surge motions predicted by the quasi-static MAP++ and the full dynamic MoorDyn. It should be noted that MoorDyn may also experience numerical instability for similar laboratory-scale physical tests (Aliyar et al., 2022; Paduano et al., 2020).

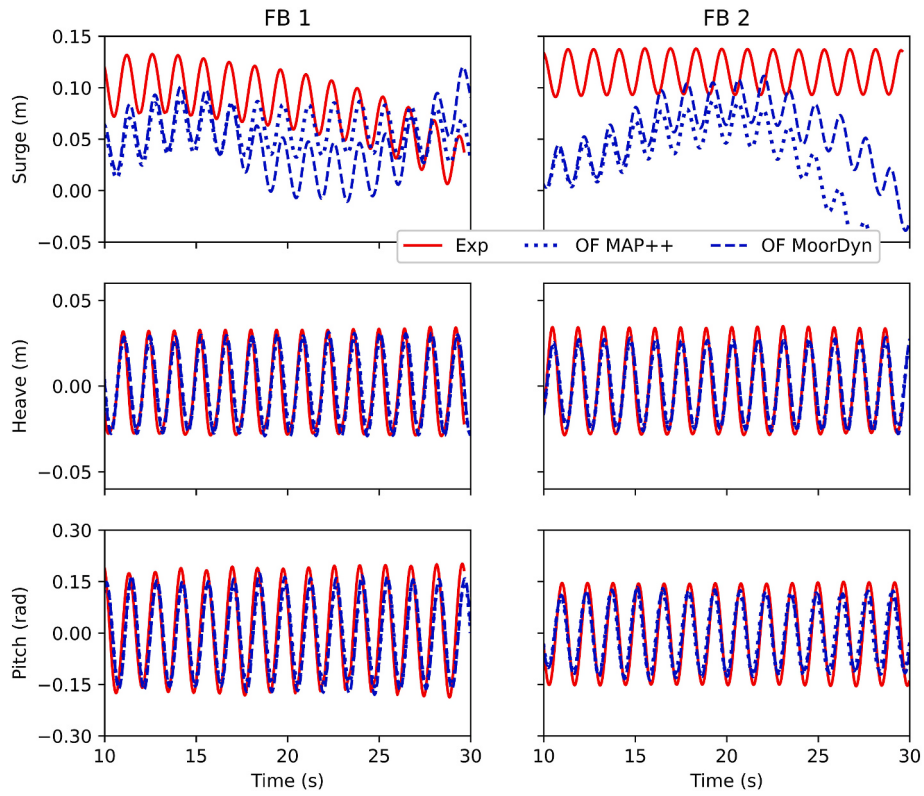


Fig. C.1. Comparison of breakwater motion predictions by three mooring codes MAP++ (dotted) and MoorDyn (dashed) for the twin FB test h05t14 (wave height 0.05 m and period 1.4 s) using OpenFOAM's rigid body dynamics library.

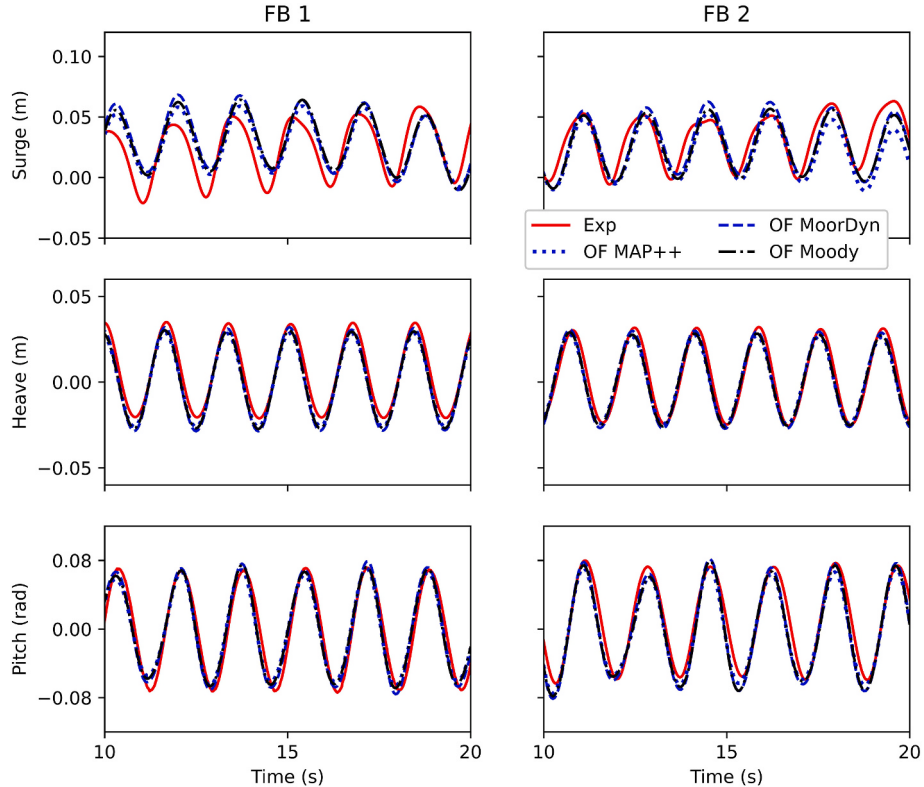


Fig. C.2. Comparison of breakwater motion predictions by three mooring codes MAP++ (dotted), MoorDyn (dashed), and Moody (dashed-dot) for the twin FB test h05t17 (wave height 0.05 m and period 1.7 s) using OpenFOAM's rigid body dynamics library.

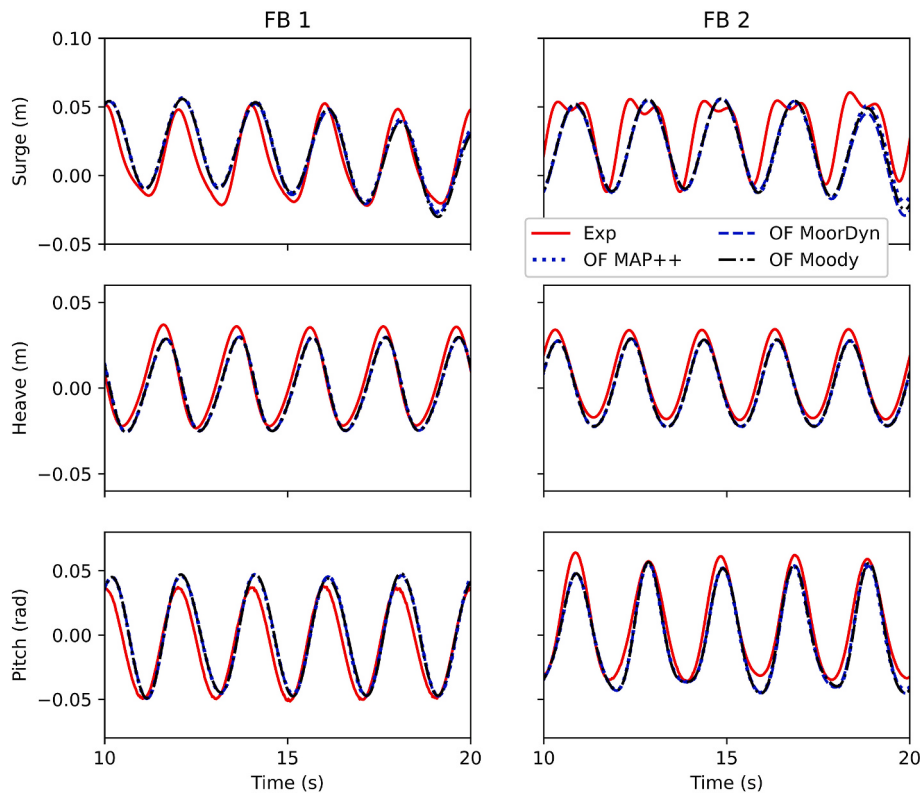


Fig. C.3. Same as Fig. C2 but for case h05t20 (wave height 0.05 m and period 2.0 s).

References

- Aliyari, S., Ducrozet, G., Bouscasse, B., Bonnefoy, F., Sriram, V., Ferrant, P., 2022. Numerical coupling strategy using HOS-OpenFOAM-MoorDyn for OC3 Hywind SPAR type platform. *Ocean Eng.* 263, 112206.
- Altomare, C., Domínguez, J.M., Crespo, A.J.C., González-Cao, J., Suzuki, T., Gómez-Gesteira, M., Troch, P., 2017. Long-crested wave generation and absorption for SPH-based DualSPHysics model. *Coast Eng.* 127, 37–54.
- Bruinsma, N., Paulsen, B.T., Jacobsen, N.G., 2018. Validation and application of a fully nonlinear numerical wave tank for simulating floating offshore wind turbines. *Ocean Eng.* 147, 647–658.
- Chen, H., Hall, M., 2022. CFD simulation of floating body motion with mooring dynamics: coupling MoorDyn with OpenFOAM. *Appl. Ocean Res.* 124, 103210.
- Chen, H., Qian, L., Ma, Z., Bai, W., Li, Y., Causon, D., Mingham, C., 2019. Application of an overset mesh based numerical wave tank for modelling realistic free-surface hydrodynamic problems. *Ocean Eng.* 176, 97–117.
- Chen, J., Zhang, J., Wang, G., Zhang, Q., Guo, J., Sun, X., 2022. Numerical simulation of the wave dissipation performance of floating box-type breakwaters under long-period waves. *Ocean Eng.* 266, 113091.
- Chen, Y.K., Liu, Y., Meringolo, D.D., Hu, J.M., 2023. Study on the hydrodynamics of a twin floating breakwater by using SPH method. *Coast Eng.* 179, 104230.
- da Fonseca, F.C., Gomes, R.P.F., Henriques, J.C.C., Gato, L.M.C., Falcão, A.F.O., 2016. Model testing of an oscillating water column spar-buoy wave energy converter isolated and in array: motions and mooring forces. *Energy* 112, 1207–1218.
- Devolder, B., Stratigaki, V., Troch, P., Rauwoens, P., 2018. CFD simulations of floating point absorber wave energy converter arrays subjected to regular waves. *Energies* 11 (3), 641.
- Domínguez, J.M., Crespo, A.J., Hall, M., Altomare, C., Wu, M., Stratigaki, V., et al., 2019. SPH simulation of floating structures with moorings. *Coast Eng.* 153, 103560.
- Dunbar, A.J., Craven, B.A., Paterson, E.G., 2015. Development and validation of a tightly coupled CFD/6-DOF solver for simulating floating offshore wind turbine platforms. *Ocean Eng.* 110, 98–105.
- Eskilsson, C., Palm, J., 2022. High-fidelity modelling of moored marine structures: multi-component simulations and fluid-mooring coupling. *Journal of Ocean Engineering and Marine Energy* 8 (4), 513–526.
- Featherstone, R., 2014. *Rigid Body Dynamics Algorithms*. Springer.
- Feng, X., Bai, W., Chen, X.B., Qian, L., Ma, Z.H., 2017. Numerical investigation of viscous effects on the gap resonance between side-by-side barges. *Ocean Eng.* 145, 44–58.
- Fredriksson, D.W., DeCew, J., Swift, M.R., Tsukrov, I., Chambers, M.D., Celikkol, B., 2004. The design and analysis of a four-cage grid mooring for open ocean aquaculture. *Aquacult. Eng.* 32 (1), 77–94.
- Gao, J., He, Z., Huang, X., Liu, Q., Zang, J., Wang, G., 2021. Effects of free heave motion on wave resonance inside a narrow gap between two boxes under wave actions. *Ocean Eng.* 224, 108753.
- Gao, J., Lyu, J., Wang, J., Zhang, J., Liu, Q., Zang, J., Zou, T., 2022. Study on transient gap resonance with consideration of the motion of floating body. *China Ocean Eng.* 36 (6), 994–1006.
- Gatin, I., Vukčević, V., Jasak, H., Rusche, H., 2017. Enhanced coupling of solid body motion and fluid flow in finite volume framework. *Ocean Eng.* 143, 295–304.
- Gomes, R.P., Gato, L.M., Henriques, J.C., Portillo, J.C., Howey, B.D., Collins, K.M., et al., 2020. Compact floating wave energy converters arrays: mooring loads and survivability through scale physical modelling. *Appl. Energy* 280, 115982.
- Guan, G., Zhang, X., Wang, Y., Yang, Q., 2021. Analytical and numerical study on underwater towing cable dynamics under different flow velocities based on experimental corrections. *Appl. Ocean Res.* 114, 102768.
- Hall, M., Goupee, A., 2015. Validation of a lumped-mass mooring line model with DeepCwind semisubmersible model test data. *Ocean Eng.* 104, 590–603.
- Han, M., Cao, F., Shi, H., Kou, H., Gong, H., Wang, C., 2023. Parametrical study on an array of point absorber wave energy converters. *Ocean Eng.* 272, 113857.
- He, G., Luan, Z., Jin, R., Zhang, W., Wang, W., Zhang, Z., et al., 2022. Numerical and experimental study on absorber-type wave energy converters concentrically arranged on an octagonal platform. *Renew. Energy* 188, 504–523.
- He, M., Liang, D., Ren, B., Li, J., Shao, S., 2023. Wave interactions with multi-float structures: SPH model, experimental validation and parametric study. *Coast Eng.*, 104333
- Higuera, P., Lara, J.L., Losada, I.J., 2013. Realistic wave generation and active wave absorption for Navier-Stokes models: application to OpenFOAM. *Coast Eng.* 71, 102–118.
- Hirt, C.W., Nichols, B.D., 1981. Volume of fluid (VOF) method for the dynamics of free boundaries. *J. Comput. Phys.* 39 (1), 201–225.
- Howey, B., Collins, K.M., Hann, M., Iglesias, G., Gomes, R.P., Henriques, J.C., et al., 2021. Compact floating wave energy converter arrays: inter-device mooring connectivity and performance. *Appl. Ocean Res.* 115, 102820.
- Huang, H., Gu, H., Chen, H.C., 2022. A new method to couple FEM mooring program with CFD to simulate Six-DoF responses of a moored body. *Ocean Eng.* 250, 110944.
- Jasak, H., 1996. Error Analysis and Estimation for the Finite Volume Method with Applications to Fluid Flows. Imperial College of Science, Technology and Medicine. Ph.D. thesis.
- Jiang, C., el Moctar, O., 2023. Extension of a coupled mooring-viscous flow solver to account for mooring-joint-multibody interaction in waves. *Journal of Ocean Engineering and Marine Energy* 9 (1), 93–111.

- Jiang, C., Xu, P., Bai, X., Zhao, Z., el Moctar, O., Zhang, G., 2023. A review of advances in modeling hydrodynamics and hydroelasticity for very large floating structures. *Ocean Eng.* 285, 115319.
- Jin, C., Bakti, F.P., Kim, M., 2020. Multi-floater-mooring coupled time-domain hydro-elastic analysis in regular and irregular waves. *Appl. Ocean Res.* 101, 102276.
- Jin, S., Wang, D., Hann, M., Collins, K., Conley, D., Greaves, D., 2023. A designed two-body hinged raft wave energy converter: from experimental study to annual power prediction for the EMEC site using WEC-Sim. *Ocean Eng.* 267, 113286.
- Jing, P., Cui, T., He, G., Zhang, C., Luan, Z., 2024. Effects of multi motion responses and incident-wave height on the gap resonances in a moonpool. *Phys. Fluids* 36 (1).
- Li, L., Ruzzo, C., Collu, M., Gao, Y., Failla, G., Arena, F., 2020. Analysis of the coupled dynamic response of an offshore floating multi-purpose platform for the Blue Economy. *Ocean Eng.* 217, 107943.
- Li, X., Xiao, Q., Zhou, Y., Ning, D., Incecik, A., Nicoll, R., et al., 2022. Coupled CFD-MBD numerical modeling of a mechanically coupled WEC array. *Ocean Eng.* 256, 111541.
- Liang, J.M., Liu, Y., Chen, Y.K., Li, A.J., 2022. Experimental study on hydrodynamic characteristics of the box-type floating breakwater with different mooring configurations. *Ocean Eng.* 254, 111296.
- Lopez-Olococ, T., Liang, G., Medina-Manuel, A., Ynocente, L.S., Jiang, Z., Souto-Iglesias, A., 2023. Experimental comparison of a dual-spar floating wind farm with shared mooring against a single floating wind turbine under wave conditions. *Eng. Struct.* 292, 116475.
- Lozon, E., Hall, M., 2023. Coupled loads analysis of a novel shared-mooring floating wind farm. *Appl. Energy* 332, 120513.
- Liu, X., Dao, M.H., Le, Q.T., 2022. A GPU-accelerated domain decomposition method for numerical analysis of nonlinear waves-current-structure interactions. *Ocean Eng.* 259, 111901.
- Ma, C., Bi, C.W., Xu, Z., Zhao, Y.P., 2022. Dynamic behaviors of a hinged multi-body floating aquaculture platform under regular waves. *Ocean Eng.* 243, 110278.
- Masciola, M., Jonkman, J., Robertson, A., 2013. Implementation of a multisegmented, quasi-static cable model. In: The Twenty-Third International Offshore and Polar Engineering Conference. International Society of Offshore and Polar Engineers. June.
- Oikonomou, C.L.G., Gomes, R.P.F., Gato, L.M.C., Falcão, A.F.O., 2020. On the dynamics of an array of spar-buoy oscillating water column devices with inter-body mooring connections. *Renew. Energy* 148, 309–325.
- Paduano, B., Giorgi, G., Gomes, R.P., Pasta, E., Henriques, J.C., Gato, L.M., Mattiazzo, G., 2020. Experimental validation and comparison of numerical models for the mooring system of a floating wave energy converter. *J. Mar. Sci. Eng.* 8 (8), 565.
- Palm, J., Eskilsson, C., Paredes, G.M., Bergdahl, L., 2016. Coupled mooring analysis for floating wave energy converters using CFD: formulation and validation. *International Journal of Marine Energy* 16, 83–99.
- Palm, J., Eskilsson, C., Bergdahl, L., 2017. An hp-adaptive discontinuous Galerkin method for modelling snap loads in mooring cables. *Ocean Eng.* 144, 266–276.
- Roenby, J., Aliyar, S., Bredmose, H., 2024. A Robust Algorithm for Computational Floating Body Dynamics. *R. Soc. Open Sci.* 11, 231453.
- Rusche, H., 2002. Computational Fluid Dynamics of Dispersed Two-phase Flows at High Phase Fractions. Imperial College. PhD thesis.
- WEC-Sim, <https://wec-sim.github.io/WEC-Sim/master/index.html>. Accessed October-23-2023.
- Wei, Y., Yu, S., Jin, P., Huang, L., Elshehbiny, K., Tezdogan, T., 2024. Coupled analysis between catenary mooring and VLFS with structural hydroelasticity in waves. *Mar. Struct.* 93, 103516.
- Weller, H.G., Tabor, G., Jasak, H., Fureby, C., 1998. A tensorial approach to computational continuum mechanics using object-oriented techniques. *Comput. Phys.* 12 (6), 620–631.
- Xu, S., Wang, S., Soares, C.G., 2019. Review of mooring design for floating wave energy converters. *Renew. Sustain. Energy Rev.* 111, 595–621.
- Yang, X., Wu, J., Xu, S., 2022. Dynamic analysis of underwater towed system under undulating motion mode of towed vehicle. *Appl. Ocean Res.* 121, 103083.
- Zeng, X., Shao, Y., Feng, X., Xu, K., Jin, R., Li, H., 2024. Nonlinear hydrodynamics of floating offshore wind turbines: A review. *Renewable and Sustainable Energy Reviews* 191, 114092.
- Zhang, D., Du, J., Yuan, Z., Yu, S., Li, H., 2023. Motion characteristics of large arrays of modularized floating bodies with hinge connections. *Phys. Fluids* 35 (7).
- Zheng, S.M., Zhang, Y.H., Zhang, Y.L., Sheng, W.A., 2015. Numerical study on the dynamics of a two-raft wave energy conversion device. *J. Fluid Struct.* 58, 271–290.
- Zhong, W., Zhao, W., Wan, D., Zhao, Y., 2024. Comparison study on mooring line models for hydrodynamic performances of floating offshore wind turbines. *Ocean Engineering* 296, 117083.